Astronomy Science Papers

George J. Bendo
University of Manchester

Outline

- Types of Science Articles
- Professional Astronomy Journals
- Finding Publications
- Paper Organization
- LaTeX
- Practical Process for Paper Writing
- Publication Statistics

Types of Science Articles

Journal articles

- Peer-reviewed
- Contain validated science results
- Used as primary reference material for other science results
- May only be fully accessible with a subscription (through a university, for example)

Monthly Notices of the ROYAL ASTRONOMICAL SOCIETY
MNRAS **463**, 252–269 (2016) doi:10.1093/mnras/stw1659
Advance Access publication 2016 July 11

Free–free and H42α emission from the dusty starburst within NGC 4945 as observed by ALMA

G. J. Bendo,[1,2]★ C. Henkel,[3,4] M. J. D'Cruze,[1] C. Dickinson,[1] G. A. Fuller[1,2] and A. Karim[5]

[1]*Jodrell Bank Centre for Astrophysics, School of Physics and Astronomy, The University of Manchester, Oxford Road, Manchester M13 9PL, UK*
[2]*UK ALMA Regional Centre Node*
[3]*Max-Planck-Institut für Radioastronomie, Auf dem Hügel 69, D-53121 Bonn, Germany*
[4]*Faculty of Science, Astronomy Department, King Abdulaziz University, PO Box 80203, Jeddah 21589, Saudi Arabia*
[5]*Argelander-Institut für Astronomie, Universität Bonn, Auf dem Hügel 71, D-53121 Bonn, Germany*

Accepted 2016 July 7. Received 2016 July 5; in original form 2016 April 7

ABSTRACT

We present observations of the 85.69 GHz continuum emission and H42α line emission from the central 30 arcsec within NGC 4945. Both sources of emission originate from nearly identical structures that can be modelled as exponential discs with scalelengths of ~2.1 arcsec (or ~40 pc). An analysis of the spectral energy distribution based on combining these data with archival data imply that 84 ± 10 per cent of the 85.69 GHz continuum emission originates from free–free emission. The electron temperature is 5400 ± 600 K, which is comparable to what has been measured near the centre of the Milky Way Galaxy. The star formation rate (SFR) based on the H42α and 85.69 GHz free–free emission (and using a distance of 3.8 Mpc) is 4.35 ± 0.25 $M_\odot$ yr^{-1}. This is consistent with the SFR from the total infrared flux and with previous measurements based on recombination line emission, and it is within a factor of ~2 of SFRs derived from radio data. The *Spitzer Space Telescope* 24 μm data and *Wide-field Infrared Survey Explorer* 22 μm data yield SFRs ~10× lower than the Atacama Large Millimeter/submillimeter Array measurements, most likely because the mid-infrared data are strongly affected by dust attenuation equivalent to $A_V = 150$. These results indicate that SFRs based on mid-infrared emission may be highly inaccurate for dusty, compact circumnuclear starbursts.

Key words: galaxies: individual: NGC 4945 – galaxies: starburst – infrared: galaxies – radio continuum: galaxies – radio lines: galaxies.

1 INTRODUCTION

The Atacama Large Millimeter/submillimeter Array (ALMA) is capable of detecting two different forms of emission from photoionized gas in the star-forming regions within other galaxies. First, ALMA can measure continuum emission at 85–100 GHz where the spectral energy distributions (SEDs) of galaxies are dominated by free–free emission (e.g. Peel et al. 2011). Second, ALMA is sensitive enough to detect recombination line emission that appears at millimetre and submillimetre wavelengths. Both free–free and millimetre recombination line emission as star formation tracers have advantages over ultraviolet, optical, and near-infrared tracers in that they are unaffected by dust attenuation. Unlike infrared or radio continuum emission, the millimetre continuum and recombination line emission directly traces photoionized gas and therefore should be more reliable for measuring accurate star formation rates (SFRs). For additional discussion about this, see Murphy et al. (2011).

Millimetre continuum observations of nearby galaxies have been relatively straightforward, but the recombination line emission has been more difficult to detect. Before ALMA, millimetre recombination lines had been detected in multiple star-forming regions within the Milky Way (e.g. Waltman et al. 1973; Wilson & Pauls 1984; Gordon 1989; Gordon & Walmsley 1990), but extragalactic millimetre recombination line emission had only been detected in M82 (Seaquist, Kerton & Bell 1994; Seaquist et al. 1996), NGC 253 (Puxley et al. 1997), and Arp 220 (Anantharamaiah et al. 2000). ALMA is capable of reaching sensitivity levels at least an order of magnitude better than other telescopes (see Remijan, Adams & Warmels 2015, for a technical review) and can therefore lead to detections in many more nearby infrared-luminous sources than was previously possible (Scoville & Murchikova 2013). At this time, however, ALMA detections of specifically recombination line emission have been limited. Bendo et al. (2015b) and Meier et al. (2015) reported the detection of millimetre recombination line emission from the nearby starburst galaxy NGC 253, and Bendo et al. (2015b) used the 99.02 GHz continuum and H40α (99.02 GHz) line emission to

★E-mail: george.bendo@manchester.ac.uk

Published by Oxford University Press on behalf of the Royal Astronomical Society

Conference proceedings

- Summaries of results presented at a conference
- Not always reviewed before publication
- Usually include results that later appear in a journal

The Spectral Energy Distribution of Galaxies
Proceedings IAU Symposium No. 284, 2011
R.J. Tuffs & C.C. Popescu, eds.

doi:10.1017/S1743921312008812

Investigations of dust heating in M81, M83 and NGC 2403 with Herschel and Spitzer

George J. Bendo[1] **and the Herschel-SPIRE Local Galaxies Guaranteed Time Programs**

[1]UK ALMA Regional Centre Node, Jodrell Bank Centre for Astrophysics
School of Physics and Astronomy, University of Manchester
Oxford Road, Manchester M13 9PL, United Kingdom
email: george.bendo@manchester.ac.uk

Abstract. We use Herschel Space Observatory and Spitzer Space Telescope 70-500 μm data along with ground-based optical and near-infrared data to understand how dust heating in the nearby face-on spiral galaxies M81, M83, and NGC 2403 is affected by the starlight from all stars and by the radiation from star-forming regions. We find that 70/160 μm flux density ratios tend to be more strongly influenced by star-forming regions. However, the 250/350 and 350/500 μm micron flux density ratios are more strongly affected by the light from the total stellar populations, suggesting that the dust emission at >250 μm originates predominantly from a component that is colder than the dust seen at <160 μm and that is relatively unaffected by star formation activity. We conclude by discussing the implications of this for modelling the spectral energy distributions of both nearby and more distant galaxies and for using far-infrared dust emission to trace star formation.

Keywords. galaxies: ISM, infrared: general

1. Introduction

After the completion of the all-sky surveys by the Infrared Astronomical Satellite, astronomers have found conflicting evidence for the heating sources of the dust producing far-infrared emission in nearby galaxies. Some authors claimed that the dust was heated primarily by star formation (e.g. Devereux & Young 1990; Buat & Xu 1996) while others indicated that evolved stellar populations could heat the dust (e.g. Sauvage & Thuan 1992; Walterbos & Greenawalt 1996). This issue has become more important since the launch of the *Herschel* Space Observatory (Pilbratt *et al.* 2010). *Herschel* has been able to produce high signal-to-noise >200 μm images of both nearby and more distant galaxies, so it will be highly sensitive to colder dust that may have been missed by telescopes primarily observing at shorter wavelengths.

Several papers have been published on the sources of the heating for the dust emitting at *Herschel* wavelengths (e.g. Bendo *et al.* 2010, Rowan-Robinson *et al.* 2010, Boquien *et al.* 2011). We will focus on the results from Bendo *et al.* (2011) on the spiral galaxies M81, M83, and NGC 2403. Their analysis was based on comparing the infrared surface brightness ratios to Hα emission (used as a tracer of star formation) and 1.6 μm emission (used as a tracer of the emission from the total stellar population). The infrared surface brightness ratios depend on dust heating, so they will appear correlated with the emission tracing the dust heating sources.

Preprints

- Pre-published versions of papers

- Usually fall into one of three categories:
    - Papers that have been accepted for publication but not yet published
    - Papers that have been submitted for publication but not yet reviewed
    - Papers that people are not going to try to submit

- Freely accessible

Mon. Not. R. Astron. Soc. 000, 1–14 () Printed 20 July 2017 (MN LaTeX style file v2.2)

Tests of star formation metrics in the low metallicity galaxy NGC 5253 using ALMA observations of H30α line emission

G. J. Bendo[1,2], R. E. Miura[3], D. Espada[3], K. Nakanishi[3,4], R. J. Beswick[1], M. J. D'Cruze[1], C. Dickinson[1], G. A. Fuller[1,2]
[1] Jodrell Bank Centre for Astrophysics, School of Physics and Astronomy, The University of Manchester, Oxford Road, Manchester M13 9PL, United Kingdom
[2] UK ALMA Regional Centre Node
[3] National Astronomical Observatory of Japan, 2-21-1 Osawa, Mitaka, Tokyo, 181-8588, Japan
[4] The Graduate University for Advanced Studies (Sokendai), 2-21-1 Osawa, Mitaka, Tokyo 181-0015, Japan

ABSTRACT
We use Atacama Large Millimeter/submillimeter Array (ALMA) observations of H30α (231.90 GHz) emission from the low metallicity dwarf galaxy NGC 5253 to measure the star formation rate (SFR) within the galaxy and to test the reliability of SFRs derived from other commonly-used metrics. The H30α emission, which originates mainly from the central starburst, yields a photoionizing photon production rate of $(1.9\pm0.3)\times10^{52}$ s^{-1} and an SFR of 0.087 ± 0.013 $M_{\odot}$ yr^{-1} based on conversions that account for the low metallicity of the galaxy and for stellar rotation. Among the other star formation metrics we examined, the SFR calculated from the total infrared flux was statistically equivalent to the values from the H30α data. The SFR based on previously-published versions of the Hα flux that were extinction corrected using Paα and Paβ lines were lower than but also statistically similar to the H30α value. The mid-infrared (22 μm) flux density and the composite star formation tracer based on Hα and mid-infrared emission give SFRs that were significantly higher because the dust emission appears unusually hot compared to typical spiral galaxies. Conversely, the 70 and 160 μm flux densities yielded SFR lower than the H30α value, although the SFRs from the 70 μm and H30α data were within 1-2σ of each other. While further analysis on a broader range of galaxies are needed, these results are instructive of the best and worst methods to use when measuring SFR in low metallicity dwarf galaxies like NGC 5253.

Key words: galaxies: dwarf - galaxies: individual: NGC 5253 - galaxies: starburst - galaxies: star formation - radio lines: galaxies

1 INTRODUCTION

Star formation in other galaxies is typically identified by looking at tracers of young stellar populations, including either photoionizing stars, ultraviolet-luminous stars, and supernovae. The most commonly-used star formation tracers are ultraviolet continuum emission; Hα (6563 Å) and other optical and near-infrared recombination lines; mid- and far-infrared continuum emission; and radio continuum emission. However, each of these tracers have disadvantages when used to measure star formation rates (SFRs). Ultraviolet continuum and optical recombination line emission directly trace the young stellar populations, but dust obscuration typically affects the SFRs from these tracers. Near-infrared recombination line emission is less affected by dust obscuration, but it is still a concern in very dusty starburst galaxies. Dust continuum emission in the infrared is unaffected by dust obscuration except in extreme cases, but since this emission is actually a tracer of bolometric stellar luminosity and not just the younger stellar population, it may yield an overestimate of the SFR if many evolved stars are present. Radio continuum emission traces a combination of free-free continuum emission from photoionized gas and synchrotron emission from supernova remnants, so proper spectral decomposition is needed to accurately convert radio emission to SFR. Additionally, the cosmic rays that produce synchrotron emission will travel significant distances through the ISM, making radio emission appear diffused relative to star formation on scales of ∼100 pc (Murphy et al. 2006a,b).

Higher-order recombination line emission at millimetre and submillimetre wavelengths, which is produced by the same photoionized gas that produce Hα and other optical and near-infrared recombination lines, can also be used to measure SFRs. Unlike ultraviolet, optical, and near-infrared star formation tracers, these millimetre and submillimetre recombination lines are not affected by dust extinction, but unlike infrared and radio synchrotron emission, the recombination lines directly trace the photoionizing stars. Recombination line emission can also be observed at centimetre and longer wavelengths, but the line emission at these longer wavelengths is generally affected by a combination of masing effects and opacity issues in the photoionized gas, while the millimetre and submillimetre lines are not (Gordon & Walmsley 1990).

Press releases

- Articles written for distribution to newspapers
- Not necessarily based on published science
- Usually not peer-reviewed

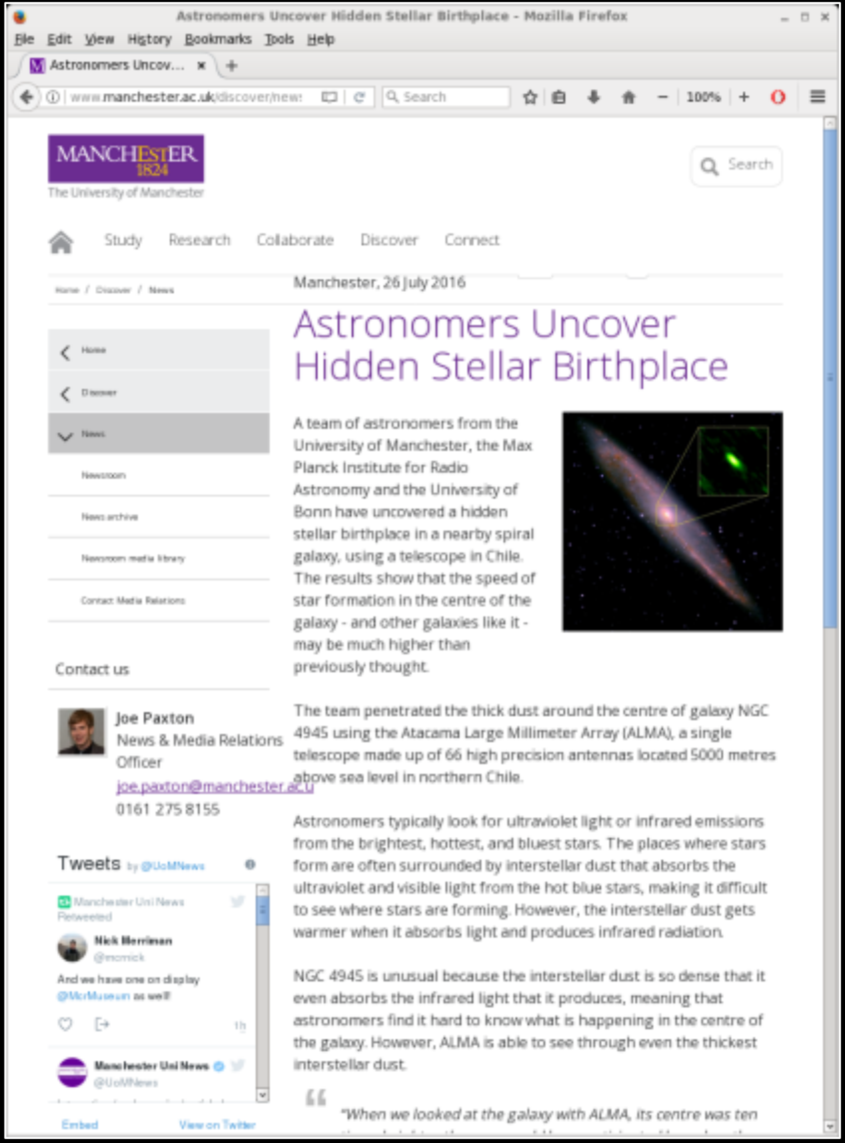

Popular science articles

- Articles written for magazines for the general public (e.g. Astronomy, Sky & Telescope)
- Not necessarily peer-reviewed
- Usually uncontroversial science

Technical papers

- Usually include support information for observatories or software
- Usually reviewed by other people in the project but not peer-reviewed
- Freely accessible

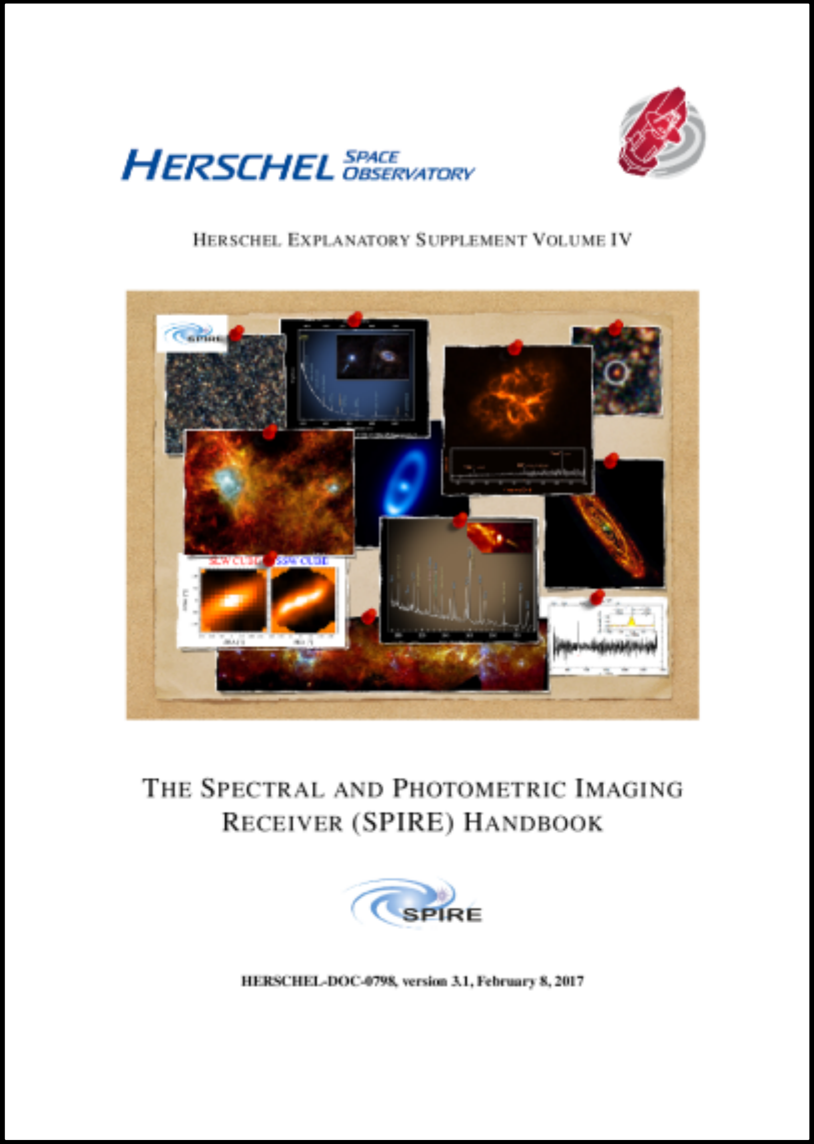

Professional Astronomy Journals

Primary astronomy journals

- Astronomical Journal
- Astronomy & Astrophysics
- Astrophysical Journal
- Monthly Notices of the Royal Astronomical Society

Astronomical Journal

AJ
iopscience.iop.org/journal/1538-3881

- The oldest American astronomy journal
- Associated with the American Astronomical Society (AAS)
- Charges for publishing
- Articles can be made open access for an additional charge

Astronomy & Astrophysics

A&A
www.aanda.org

- Europe’s main astronomy journal
- Free to publish for people in the UK (except for excessively long papers)
- Articles become open access one year after publication

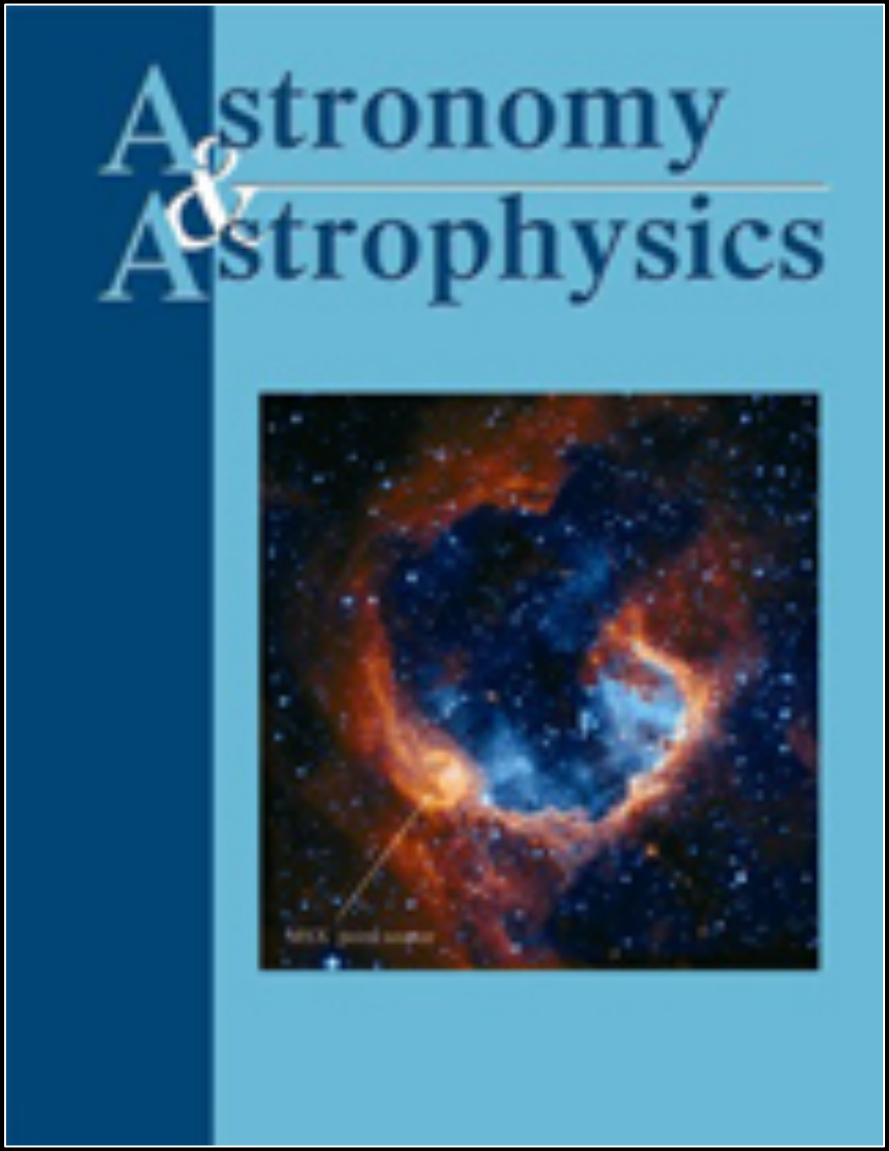

Astrophysical Journal

ApJ
iopscience.iop.org/journal/0004-637X

- The most highly cited main astronomy journal
- Associated with the American Astronomical Society (AAS)
- Charges for publishing
- Articles can be made open access for an additional charge

Monthly Notices of the Royal Astronomical Society

MNRAS
academic.oup.com/mnras

- The main astronomy journal for the United Kingdom
- Associated with the Royal Astronomical Society (RAS)
- Charges for publishing colour figures in the print version
- Articles can be made open access for an additional charge

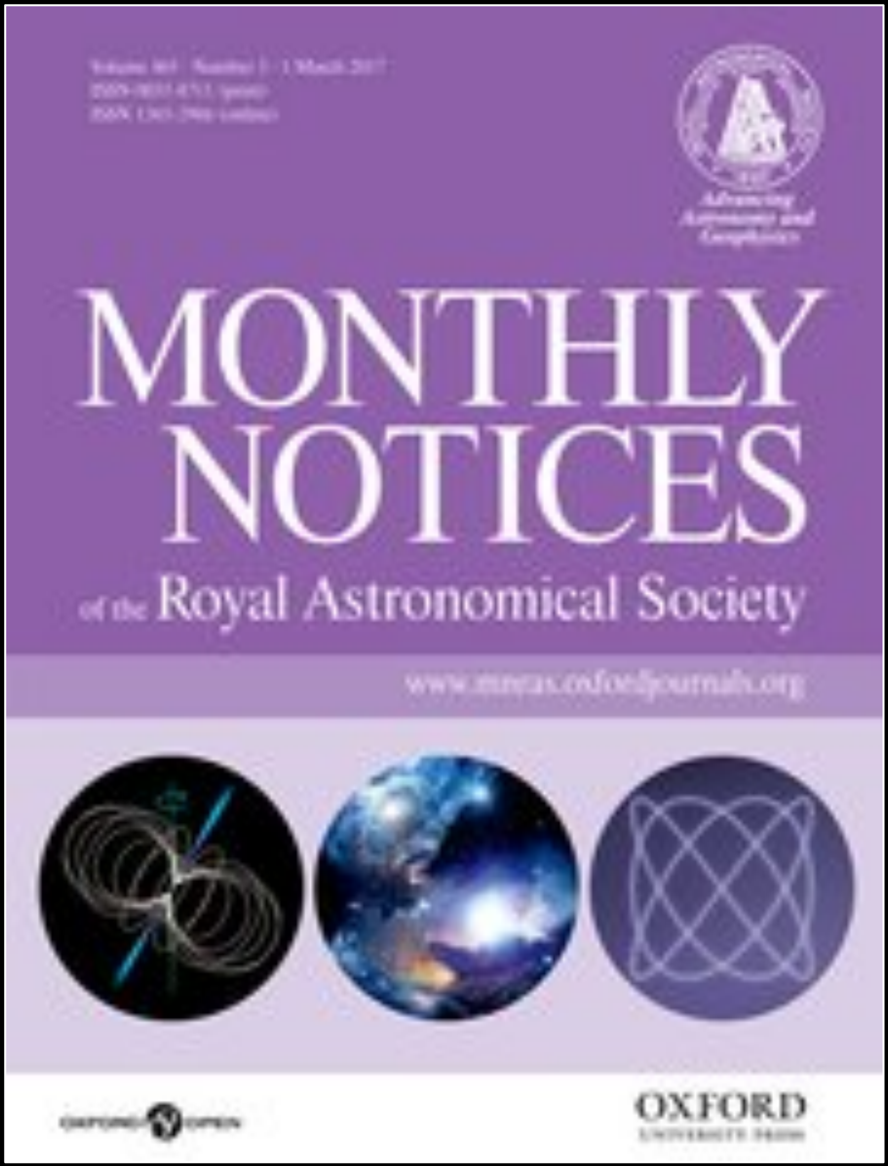

Other astronomy-related journals

(not a complete list)

- **Annual Review of Astronomy & Astrophysics (*ARA&A*)** – A good source for overview information on research topics
- **Icarus** – A journal oriented towards planetary astronomy
- **Nature** – A journal covering a broad range of sciences that published high-profile results (including astronomy results)
- **Publications of the Astronomical Society of Japan (*PASJ*)** – Japan's main astronomy journal
- **Publications of the Astronomical Society of the Pacific (*PASP*)** – Often used to present background information on surveys
- **Science** – Another journal covering a broad range of sciences that published high-profile results

Variants of the main journals

- **Letters** – Short articles that are published on a short timescale; used to highlight new results without providing in-depth information

- **Supplements** – Used to publish large datasets

Fake or questionable journals

Some legitimate journals not listed above deal with specialty topics or are focused on fields other than astronomy. However, beware of “journals” that do not appear on this list and that are unfamiliar to your supervisor.

Some other signs that an astronomy journal may either be fake or otherwise questionable:

- You receive email requests from the journal for articles.
- You receive email requests from the journal to be a guest editor.
- The journal is never cited in any scientific papers that you read.
- No one at your university has published in the journal.
- No one at your university has heard of the journal.
- The journal has not been around for more than 10 years.
- The journal is not associated with a major research organization.
- The journal’s editorial board is either not shown or consists of relatively unknown people.

Finding Publications

ADS Abstracts

In the mid-1990s, astronomers set up the ADS Abstracts website to catalogue all professional astronomy publications.

The website is accessible at adswww.harvard.edu/ads_abstracts.html .

Try looking up the webpage now.

The original version of the website is at adsabs.harvard.edu/abstract_service.html .

This has fields for searching for the following:

- Author
- Object name
- Title words
- Abstract words

The form also has multiple options for narrowing down the search or sorting the results.

The results can be sorted afterwards.

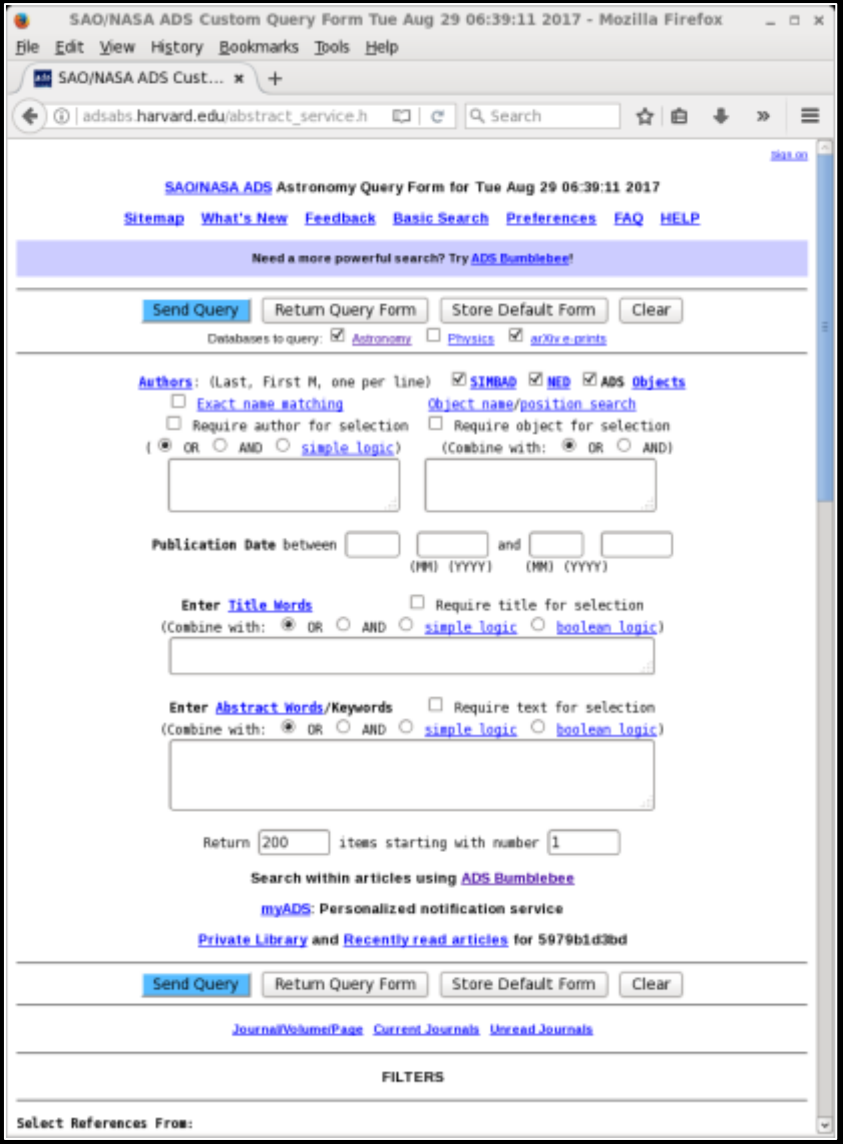

The original version of the website is at adsabs.harvard.edu/abstract_service.html .

This has fields for searching for the following:

- Author
- Object name
- Title words
- Abstract words

The form also has multiple options for narrowing down the search or sorting the results.

The results can be sorted afterwards.

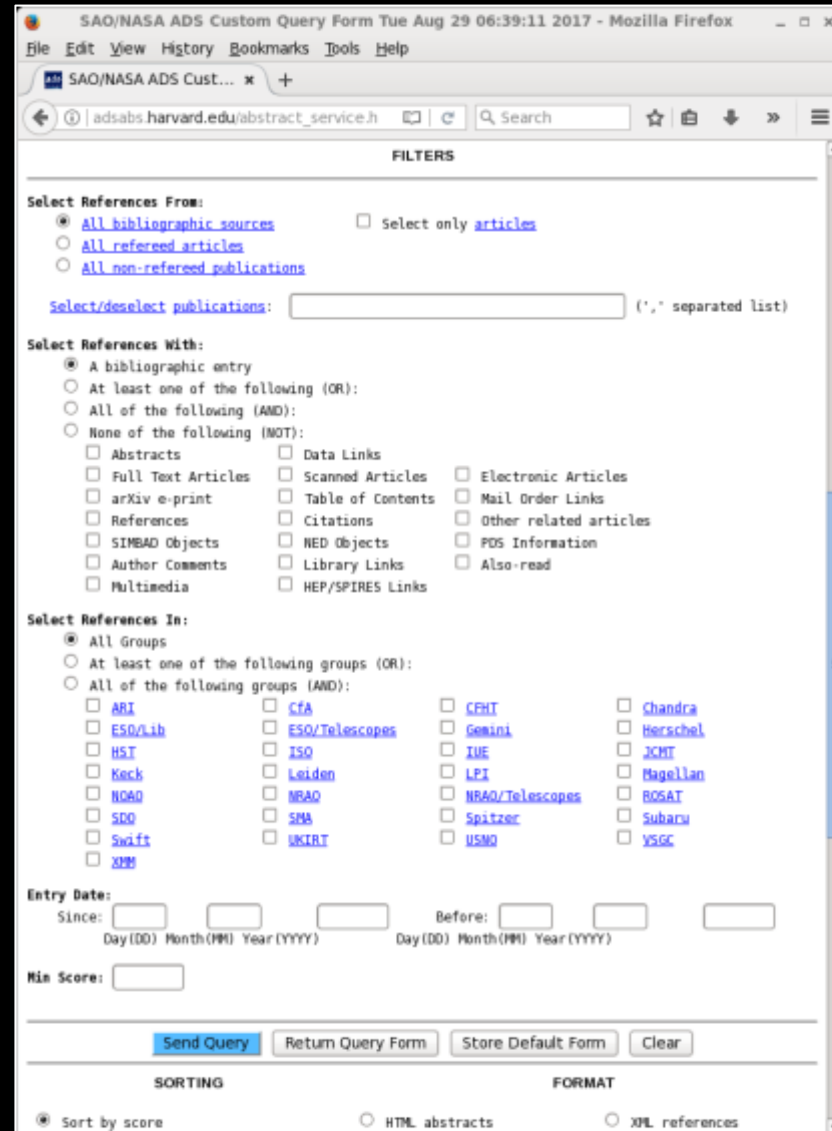

The original version of the website is at adsabs.harvard.edu/abstract_service.html .

This has fields for searching for the following:

- Author
- Object name
- Title words
- Abstract words

The form also has multiple options for narrowing down the search or sorting the results.

The results can be sorted afterwards.

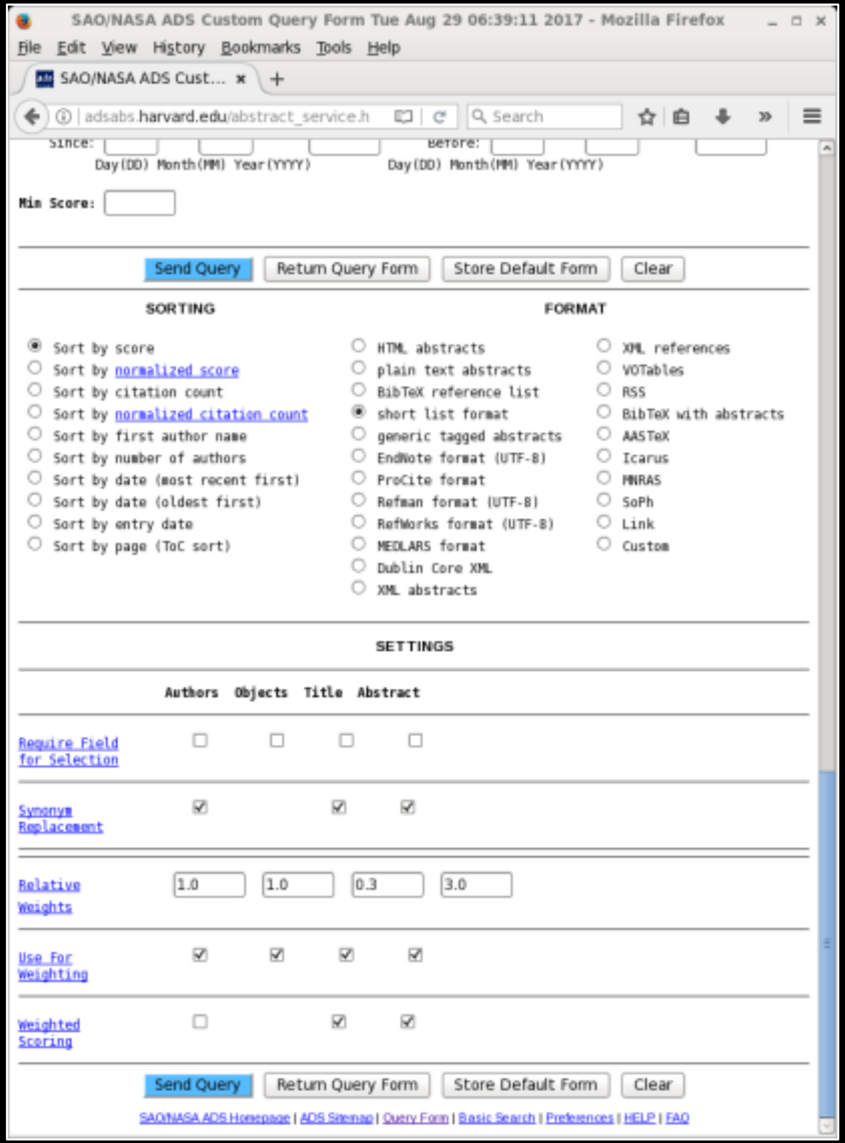

The new version of the website is at ui.adsabs.harvard.edu .

This has one entry field, but it is possible to perform multiple types of queries.

The list of results can be filtered afterwards.

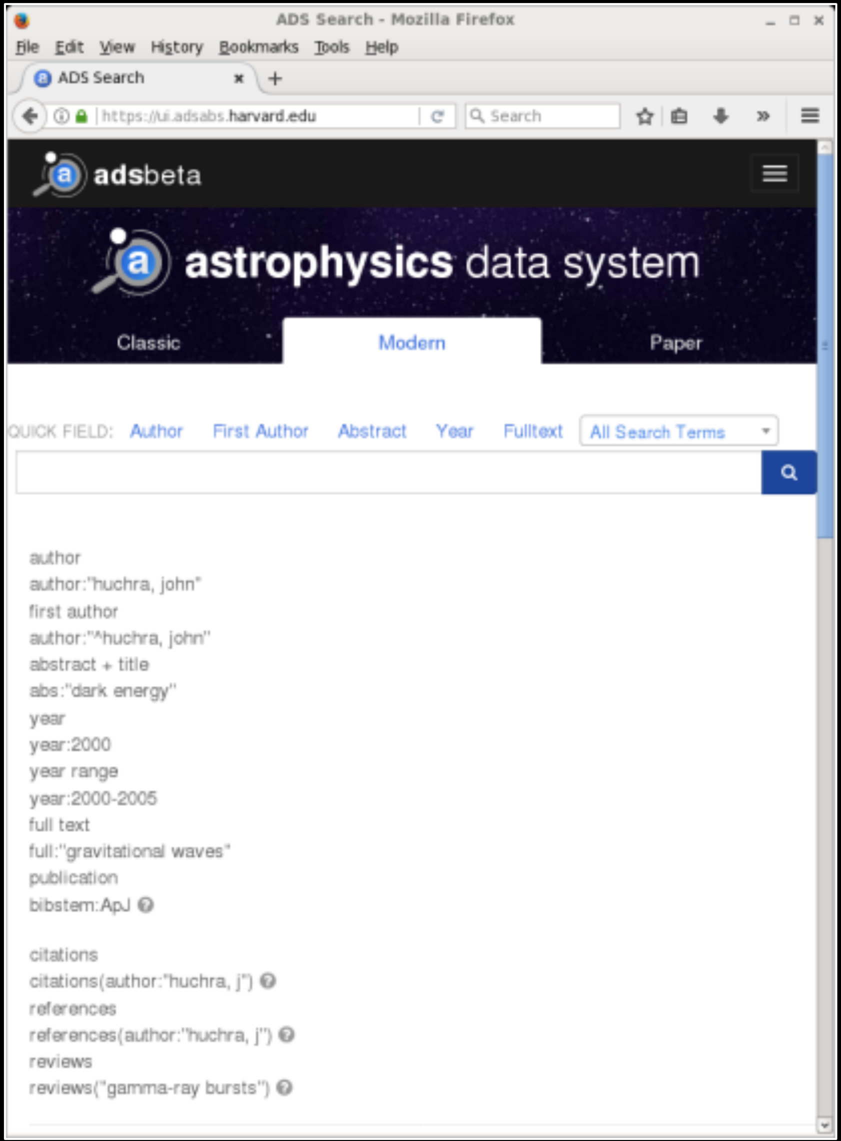

Tips on using ADS Abstracts

- To search for first-author papers, use a “^” in front of the name (for example, “^Smith”).
- To search for last-author papers, uise a “$” after the name (for example, “Smith$”).
- With very common names, it may be useful to use the Boolean logic options to remove some entries with initials that do not quite match.
- In the classic form, using the “and” options will limit the total number of results.
- When filling in multiple input fields in the classic form, it is important to check the “Require for selection” boxes.
- Filtering by refereed articles is often useful for reducing the number of results.

arXiv

The arXiv website at arxiv.org carries preprints of many journal articles and some conference proceedings.

Some people also use it to “publish” results when they cannot get their articles accepted by any journals.

The new submissions list is updated every weekday. Some people use this list to keep up on astronomy research.

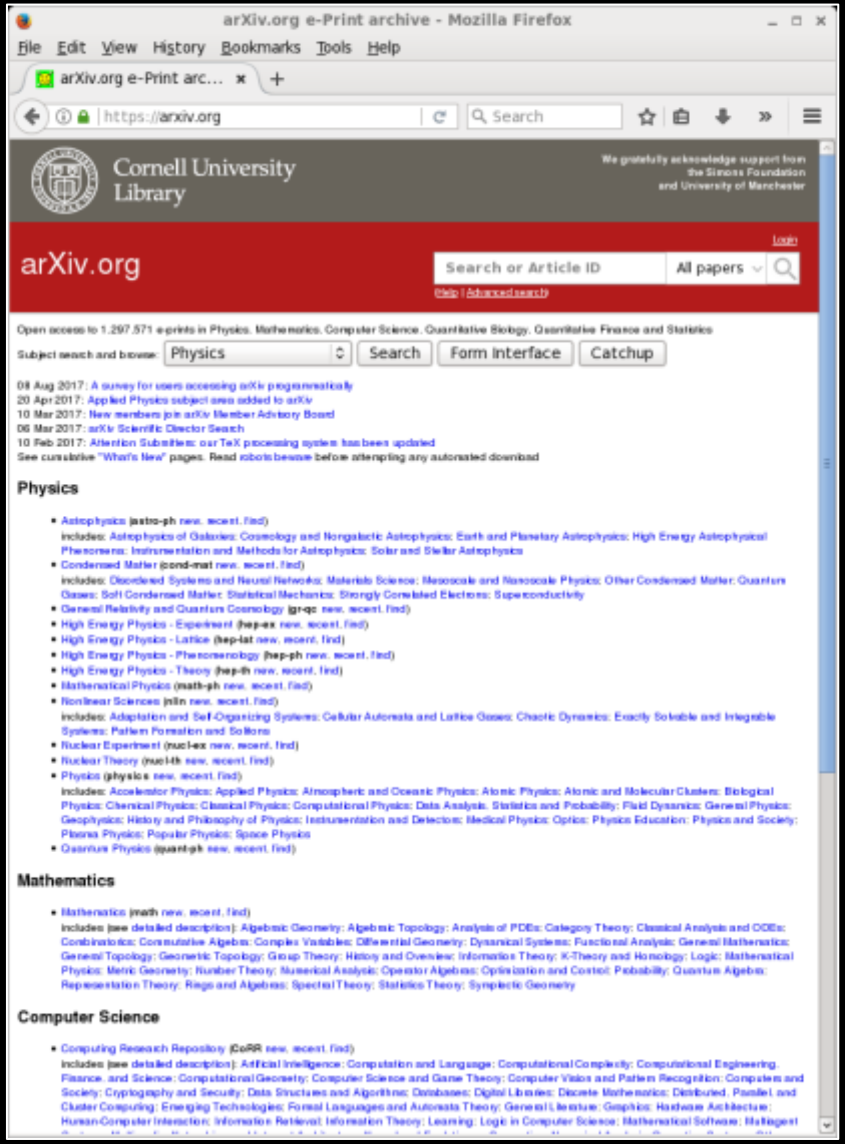

arXiv

The arXiv website at arxiv.org carries preprints of many journal articles and some conference proceedings.

Some people also use it to “publish” results when they cannot get their articles accepted by any journals.

The new submissions list is updated every weekday. Some people use this list to keep up on astronomy research.

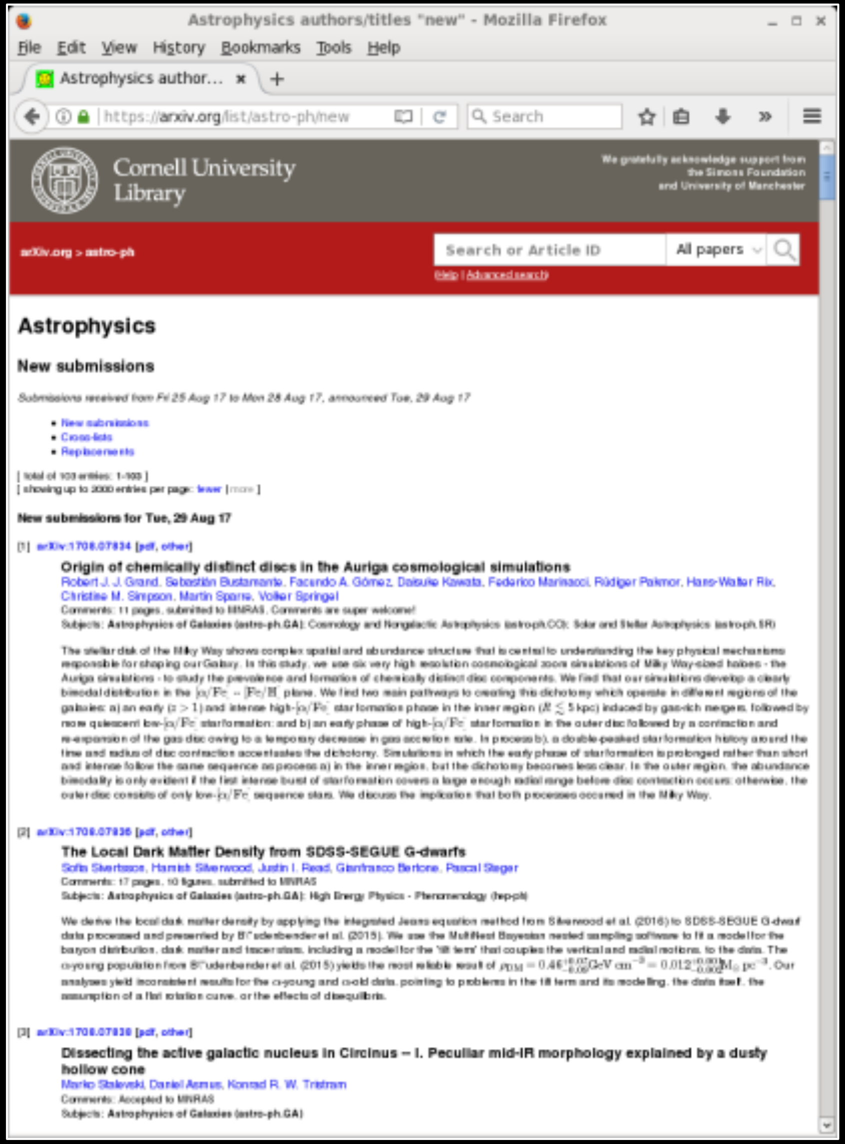

Paper Organization

Astronomy papers are generally organized along the following outline:

- Introduction
- Data
- Analysis
- Discussion
- Conclusions

However, many papers will frequently reorganize the material in unusual or creative ways. It is rare to actually see a paper with five sections with these labels.

Title

The paper begins with the title.

The title should communicate what the paper is about as briefly as possible.

However, you can have fun with making creative titles.


Monthly Notices of the Royal Astronomical Society

MNRAS 463, 252–269 (2016)

doi:10.1093/mnras/stw1659

Free–free and H42α emission from the dusty starburst within NGC 4945 as observed by ALMA

and A. Karim[5]

Accepted 2016 July 7. Received 2016 July 5; in original form 2016 April 7

ABSTRACT

We present observations of the 85.69 GHz continuum emission and H42α line emission from the central 30 arcsec within NGC 4945. Both sources of emission originate from nearly identical structures that can be modelled as exponential discs with scalelengths of ∼2.1 arcsec (or ∼40 pc). An analysis of the spectral energy distribution based on combining these data with archival data imply that 84 ± 10 per cent of the 85.69 GHz continuum emission originates from free–free emission. The electron temperature is 5400 ± 600 K, which is comparable to what has been measured near the centre of the Milky Way Galaxy. The star formation rate (SFR) based on the H42α and 85.69 GHz free–free emission (and using a distance of 3.8 Mpc) is 4.35 ± 0.25 $M_{\odot}$ yr^{-1}. This is consistent with the SFR from the total infrared flux and with previous measurements based on recombination line emission, and it is within a factor of ∼2 of SFRs derived from radio data. The *Spitzer Space Telescope* 24 μm data and *Wide-field Infrared Survey Explorer* 22 μm data yield SFRs ∼10× lower than the Atacama Large Millimeter/submillimeter Array measurements, most likely because the mid-infrared data are strongly affected by dust attenuation equivalent to A_V = 150. These results indicate that SFRs based on mid-infrared emission may be highly inaccurate for dusty, compact circumnuclear starbursts.

Key words: galaxies: individual: NGC 4945 – galaxies: starburst – infrared: galaxies – radio continuum: galaxies – radio lines: galaxies.

1 INTRODUCTION

© 2016 The Authors

Published by Oxford University Press on behalf of the Royal Astronomical Society

Author list

Underneath the title is the author list (as well as a list of everyone's affiliations).

Including every possible contributor in the author list in important to ensure that everyone's contribution is acknowledged.

However, some author lists can get inanely long.

Monthly Notices of the ROYAL ASTRONOMICAL SOCIETY

MNRAS 463, 252–269 (2016) doi:10.1093/mnras/stw1659
Advance Access publication 2016 July 11

Free–free and H42α emission from the dusty starburst within NGC 4945

G. J. Bendo,[1,2★] C. Henkel,[3,4] M. J. D'Cruze,[1] C. Dickinson,[1] G. A. Fuller[1,2] and A. Karim[5]

[1] *Jodrell Bank Centre for Astrophysics, School of Physics and Astronomy, The University of Manchester, Oxford Road, Manchester M13 9PL, UK*
[2] *UK ALMA Regional Centre Node*
[3] *Max-Planck-Institut für Radioastronomie, Auf dem Hügel 69, D-53121 Bonn, Germany*
[4] *Faculty of Science, Astronomy Department, King Abdulaziz University, PO Box 80203, Jeddah 21589, Saudi Arabia*
[5] *Argelander-Institut für Astronomie, Universität Bonn, Auf dem Hügel 71, D-53121 Bonn, Germany*

Accepted 2016 July 7. Received 2016 July 5; in original form 2016 April 7

ABSTRACT

We present observations of the 85.69 GHz continuum emission and H42α line emission from the central 30 arcsec within NGC 4945. Both sources of emission originate from nearly identical structures that can be modelled as exponential discs with scalelengths of ~2.1 arcsec (or ~40 pc). An analysis of the spectral energy distribution based on combining these data with archival data imply that 84 ± 10 per cent of the 85.69 GHz continuum emission originates from free–free emission. The electron temperature is 5400 ± 600 K, which is comparable to what has been measured near the centre of the Milky Way Galaxy. The star formation rate (SFR) based on the H42α and 85.69 GHz free–free emission (and using a distance of 3.8 Mpc) is 4.35 ± 0.25 $M_\odot$ yr^{-1}. This is consistent with the SFR from the total infrared flux and with previous measurements based on recombination line emission, and it is within a factor of ~2 of SFRs derived from radio data. The *Spitzer Space Telescope* 24 μm data and *Wide-field Infrared Survey Explorer* 22 μm data yield SFRs ~10× lower than the Atacama Large Millimeter/submillimeter Array measurements, most likely because the mid-infrared data are strongly affected by dust attenuation equivalent to $A_V = 150$. These results indicate that SFRs based on mid-infrared emission may be highly inaccurate for dusty, compact circumnuclear starbursts.

Key words: galaxies: individual: NGC 4945 – galaxies: starburst – infrared: galaxies – radio continuum: galaxies – radio lines: galaxies.

1 INTRODUCTION

The Atacama Large Millimeter/submillimeter Array (ALMA) is capable of detecting two different forms of emission from photoionized gas in the star-forming regions within other galaxies. First, ALMA can measure continuum emission at 85–100 GHz where the spectral energy distributions (SEDs) of galaxies are dominated by free–free emission (e.g. Peel et al. 2011). Second, ALMA is sensitive enough to detect recombination line emission that appears at millimetre and submillimetre wavelengths. Both free–free and millimetre recombination line emission as star formation tracers have advantages over ultraviolet, optical, and near-infrared tracers in that they are unaffected by dust attenuation. Unlike infrared or radio continuum emission, the millimetre continuum and recombination line emission directly traces photoionized gas and therefore should be more reliable for measuring accurate star formation rates (SFRs). For additional discussion about this, see Murphy et al. (2011).

Millimetre continuum observations of nearby galaxies have been relatively straightforward, but the recombination line emission has been more difficult to detect. Before ALMA, millimetre recombination lines had been detected in multiple star-forming regions within the Milky Way (e.g. Waltman et al. 1973; Wilson & Pauls 1984; Gordon 1989; Gordon & Walmsley 1990), but extragalactic millimetre recombination line emission had only been detected in M82 (Seaquist, Kerton & Bell 1994; Seaquist et al. 1996), NGC 253 (Puxley et al. 1997), and Arp 220 (Anantharamaiah et al. 2000). ALMA is capable of reaching sensitivity levels at least an order of magnitude better than other telescopes (see Remijan, Adams & Warmels 2015, for a technical review) and can therefore lead to detections in many more nearby infrared-luminous sources than was previously possible (Scoville & Murchikova 2013). At this time, however, ALMA detections of specifically recombination line emission have been limited. Bendo et al. (2015b) and Meier et al. (2015) reported the detection of millimetre recombination line emission from the nearby starburst galaxy NGC 253, and Bendo et al. (2015b) used the 99.02 GHz continuum and H40α (99.02 GHz) line emission to

★ E-mail: george.bendo@manchester.ac.uk

Author list

Underneath the title is the author list (as well as a list of everyone's affiliations).

Including every possible contributor in the author list in important to ensure that everyone's contribution is acknowledged.

However, some author lists can get inanely long.

Mon. Not. R. Astron. Soc. 316, 315–325 (2000)

The line-of-sight velocity distributions of simulated merger remnants

George J. Bendo* and Joshua E. Barnes
Institute for Astronomy, 2680 Woodlawn Drive, Honolulu, HI 96822, USA

Accepted 2000 February 23. Received 2000 January 4; in original form 1999 November 2

ABSTRACT

We use Gauss–Hermite functions to study the line-of-sight velocity distributions in simulated merger remnants. Our sample contains 16 remnants; eight produced by mergers between disc galaxies of equal mass, and eight produced by mergers between disc galaxies with mass ratios of 3:1. The equal-mass mergers display a wide range of kinematic features, including counterrotation at large radii, orthogonally rotating cores and misaligned rotational axes. Most of the unequal-mass remnants exhibit fairly regular disc-like kinematics, although two have kinematics more typical of the equal-mass remnants. Our results may be compared with observations of early-type objects, including ellipticals with misaligned kinematic axes, counterrotating systems and S0 galaxies.

Key words: galaxies: elliptical and lenticular, cD – galaxies: interactions – galaxies: kinematics and dynamics – galaxies: spiral.

1 INTRODUCTION

Kinematic studies of early-type galaxies have revealed a remarkable variety of interesting behaviour; some galaxies have rotation axes 'misaligned' with respect to their minor axes (Franx, Illingworth & de Zeeuw 1991), while in others the inner regions counterrotate with respect to the rest of the galaxy (Bender & Surma 1992; van der Marel & Franx 1993; Statler, Smecker-Hane & Cecil 1996). Such intriguing kinematics could plausibly result if these galaxies are the end-products of disc–galaxy mergers (Toomre & Toomre 1972), and *N*-body simulations have gone some way towards showing that mergers can indeed produce remnants with distinctive kinematics (Hernquist & Barnes 1991; Barnes 1992, 1998; Balcells & González 1998). However, other theories have been put forward for such kinematic features, particularly in the case of counterrotation (Kormendy 1984; Bertola, Buson & Zeilinger 1988; Balcells 1991). Distinguishing between major mergers and other explanations for distinctive kinematics in galaxies has been especially difficult.

The projected luminosity profiles and isophotal shapes of simulated disc galaxy mergers are reasonably good matches to those of elliptical galaxies (e.g. Barnes 1988; Hernquist 1992, 1993; Governato, Reduzzi & Rampazzo 1993; Heyl, Hernquist & Spergel 1994), but few workers have investigated the projected *kinematics* of simulated merger remnants. Hernquist (1992, 1993) described principal-axis profiles of projected mean velocity and velocity dispersion for several disc–disc merger remnants, and Heyl, Hernquist & Spergel (1996) studied line-of-sight velocity distributions for a somewhat larger sample of objects. These studies showed that kinematic misalignments of merger remnants are observable, and indicated that skewness of line profiles could provide information on the initial orientations of the merging discs. However, while systematically exploring different projections, these studies were limited to equal-mass mergers, and did not examine the structure of line profiles in detail or map velocity fields in two dimensions.

Therefore we studied line-of-sight velocity distributions for a larger sample of simulated merger remnants. We examined eight mergers between disc galaxies with mass ratios of 1:1, and another eight mergers between disc galaxies with mass ratios of 3:1. We limited our analysis to a single projection along the intermediate axis of each remnant, but we complement an extensive presentation of major-axis kinematics with detailed examinations of individual line profiles and with two-dimensional maps of key kinematic parameters. This work extends the studies described above to unequal-mass mergers, clarifies the connection between initial conditions and line profile, and provides predictions to be compared with kinematic studies of early-type galaxies using the next generation of integral-field spectrometers.

The outline of this paper is as follows. The rest of Section 1 describes the merger simulations and the methods we use to extract line-of-sight velocity distributions and represent the distributions with Gauss–Hermite parameters. Sections 2 and 3 present the results for the equal-mass and unequal-mass mergers, respectively. Section 4 compares our results to observational studies and summarizes our conclusions.

1.1 Merger simulations

The remnants analysed here came from a modest survey of parabolic encounters between model disc galaxies (Barnes 1998). Each model had three components: a central bulge with a shallow cusp (Hernquist 1990), an exponential/isothermal disc with

* E-mail: bendo@ifa.hawaii.edu

Author list

Underneath the title is the author list (as well as a list of everyone's affiliations).

Including every possible contributor in the author list in important to ensure that everyone's contribution is acknowledged.

However, some author lists can get inanely long.


A&A 582, A28 (2015)
DOI: 10.1051/0004-6361/201424643
© ESO 2015

Astronomy & Astrophysics

Planck intermediate results

Planck Collaboration: P. A. R. Ade, N. Aghanim, M. Arnaud, M. Ashdown, J. Aumont, C. Baccigalupi, A. J. Banday, R. B. Barreiro, N. Bartolo, E. Battaner, R. Battye, K. Benabed, G. J. Bendo, A. Benoit-Lévy, J.-P. Bernard, M. Bersanelli, P. Bielewicz, A. Bonaldi, L. Bonavera, J. R. Bond, J. Borrill, F. R. Bouchet, C. Burigana, R. C. Butler, E. Calabrese, J.-F. Cardoso, A. Catalano, A. Chamballu, R.-R. Chary, X. Chen, H. C. Chiang, P. R. Christensen, D. L. Clements, L. P. L. Colombo, C. Combet, F. Couchot, A. Coulais, B. P. Crill, A. Curto, F. Cuttaia, L. Danese, R. D. Davies, R. J. Davis, P. de Bernardis, A. de Rosa, G. de Zotti, J. Delabrouille, C. Dickinson, J. M. Diego, H. Dole, S. Donzelli, O. Doré, M. Douspis, A. Ducout, X. Dupac, G. Efstathiou, F. Elsner, T. A. Enßlin, H. K. Eriksen, F. Finelli, O. Forni, M. Frailis, A. A. Fraisse, E. Franceschi, A. Frejsel, S. Galeotta, K. Ganga, M. Giard, Y. Giraud-Héraud, E. Gjerløw, J. González-Nuevo, K. M. Górski, A. Gregorio, A. Gruppuso, F. K. Hansen, D. Hanson, D. L. Harrison, S. Henrot-Versillé, C. Hernández-Monteagudo, D. Herranz, S. R. Hildebrandt, E. Hivon, M. Hobson, W. A. Holmes, A. Hornstrup, W. Hovest, K. M. Huffenberger, G. Hurier, F. P. Israel, A. H. Jaffe, T. R. Jaffe, W. C. Jones, M. Juvela, E. Keihänen, R. Keskitalo, T. S. Kisner, R. Kneissl, J. Knoche, M. Kunz, H. Kurki-Suonio, G. Lagache, A. Lähteenmäki, J.-M. Lamarre, A. Lasenby, M. Lattanzi, C. R. Lawrence, R. Leonardi, F. Levrier, M. Liguori, P. B. Lilje, M. Linden-Vørnle, M. López-Caniego, P. M. Lubin, J. F. Macías-Pérez, S. Madden, B. Maffei, D. Maino, N. Mandolesi, M. Maris, P. G. Martin, E. Martínez-González, S. Masi, S. Matarrese, P. Mazzotta, L. Mendes, A. Mennella, M. Migliaccio, M.-A. Miville-Deschênes, A. Moneti, L. Montier, G. Morgante, D. Mortlock, D. Munshi, J. A. Murphy, P. Naselsky, F. Nati, P. Natoli, H. U. Nørgaard-Nielsen, F. Noviello, D. Novikov, I. Novikov, C. A. Oxborrow, L. Pagano, F. Pajot, R. Paladini, D. Paoletti, B. Partridge, F. Pasian, T. J. Pearson, M. Peel*, O. Perdereau, F. Perrotta, V. Pettorino, F. Piacentini, M. Piat, E. Pierpaoli, D. Pietrobon, S. Plaszczynski, E. Pointecouteau, G. Polenta, L. Popa, G. W. Pratt, S. Prunet, J.-L. Puget, J. P. Rachen, M. Reinecke, M. Remazeilles, C. Renault, S. Ricciardi, I. Ristorcelli, G. Rocha, C. Rosset, M. Rossetti, G. Roudier, J. A. Rubiño-Martín, B. Rusholme, M. Sandri, G. Savini, D. Scott, L. D. Spencer, V. Stolyarov, R. Sudiwala, D. Sutton, A.-S. Suur-Uski, J.-F. Sygnet, J. A. Tauber, L. Terenzi, L. Toffolatti, M. Tomasi, M. Tristram, M. Tucci, G. Umana, L. Valenziano, J. Valiviita, B. Van Tent, P. Vielva, F. Villa, L. A. Wade, B. D. Wandelt, R. Watson, I. K. Wehus, D. Yvon, A. Zacchei, and A. Zonca

(Affiliations can be found after the references)

ABSTRACT

The Andromeda galaxy (M 31) is one of a few galaxies that has sufficient angular size on the sky to be resolved by the *Planck* satellite. *Planck* has detected M 31 in all of its frequency bands, and has mapped out the dust emission with the High Frequency Instrument, clearly resolving multiple spiral arms and sub-features. We examine the morphology of this long-wavelength dust emission as seen by *Planck*, including a study of its outermost spiral arms, and investigate the dust heating mechanism across M 31. We find that dust dominating the longer wavelength emission ($\gtrsim$0.3 mm) is heated by the diffuse stellar population (as traced by 3.6 μm emission), with the dust dominating the shorter wavelength emission heated by a mix of the old stellar population and star-forming regions (as traced by 24 μm emission). We also fit spectral energy distributions for individual 5′ pixels and quantify the dust properties across the galaxy, taking into account these different heating mechanisms, finding that there is a linear decrease in temperature with galactocentric distance for dust heated by the old stellar population, as would be expected, with temperatures ranging from around 22 K in the nucleus to 14 K outside of the 10 kpc ring. Finally, we measure the integrated spectrum of the whole galaxy, which we find to be well-fitted with a global dust temperature of (18.2 ± 1.0) K with a spectral index of 1.62 ± 0.11 (assuming a single modified blackbody), and a significant amount of free-free emission at intermediate frequencies of 20–60 GHz, which corresponds to a star formation rate of around 0.12 $M_\odot\,yr^{-1}$. We find a 2.3σ detection of the presence of spinning dust emission, with a 30 GHz amplitude of 0.7 ± 0.3 Jy, which is in line with expectations from our Galaxy.

Key words. galaxies: individual: Messier 31 – galaxies: structure – galaxies: ISM – submillimeter: galaxies – radio continuum: galaxies

* Corresponding author: M. Peel, email@mikepeel.net

Article published by EDP Sciences

A28, page 1 of 23

Abstract

The abstract provides a short summary of the paper.

This might be the only thing that people every read from your paper.

Ensure that you present all of your most important results in as few words as possible.

Monthly Notices of the Royal Astronomical Society

MNRAS 463, 252–269 (2016) doi:10.1093/mnras/stw1659
Advance Access publication 2016 July 11

Free–free and H42α emission from the dusty starburst within NGC 4945 as observed by ALMA

G. J. Bendo,[1,2]★ C. Henkel,[3,4] M. J. D'Cruze,[1] C. Dickinson,[1] G. A. Fuller[1,2] and A. Karim[5]

[1] *Jodrell Bank Centre for Astrophysics, School of Physics and Astronomy, The University of Manchester, Oxford Road, Manchester M13 9PL, UK*
[2] *UK ALMA Regional Centre Node*
[3] *Max-Planck-Institut für Radioastronomie, Auf dem Hügel 69, D-53121 Bonn, Germany*
[4] *Faculty of Science, Astronomy Department, King Abdulaziz University, PO Box 80203, Jeddah 21589, Saudi Arabia*
[5] *Argelander-Institut für Astronomie, Universität Bonn, Auf dem Hügel 71, D-53121 Bonn, Germany*

Accepted 2016 July 7. Received 2016 July 5; in original form 2016 April 7

ABSTRACT

We present observations of the 85.69 GHz continuum emission and H42α line emission from the central 30 arcsec within NGC 4945. Both sources of emission originate from nearly identical structures that can be modelled as exponential discs with scalelengths of ~2.1 arcsec (or ~40 pc). An analysis of the spectral energy distribution based on combining these data with archival data imply that 84 ± 10 per cent of the 85.69 GHz continuum emission originates from free–free emission. The electron temperature is 5400 ± 600 K, which is comparable to what has been measured near the centre of the Milky Way Galaxy. The star formation rate (SFR) based on the H42α and 85.69 GHz free–free emission (and using a distance of 3.8 Mpc) is 4.35 ± 0.25 $M_{\odot}$ yr^{-1}. This is consistent with the SFR from the total infrared flux and with previous measurements based on recombination line emission, and it is within a factor of ~2 of SFRs derived from radio data. The *Spitzer Space Telescope* 24 μm data and *Wide-field Infrared Survey Explorer* 22 μm data yield SFRs ~10× lower than the Atacama Large Millimeter/submillimeter Array measurements, most likely because the mid-infrared data are strongly affected by dust attenuation equivalent to $A_V = 150$. These results indicate that SFRs based on mid-infrared emission may be highly inaccurate for dusty, compact circumnuclear starbursts.

continuum: galaxies – radio lines: galaxies.

1 INTRODUCTION

The Atacama Large Millimeter/submillimeter Array (ALMA) is capable of detecting two different forms of emission from photoionized gas in the star-forming regions within other galaxies. First, ALMA can measure continuum emission at 85–100 GHz where the spectral energy distributions (SEDs) of galaxies are dominated by free–free emission (e.g. Peel et al. 2011). Second, ALMA is sensitive enough to detect recombination line emission that appears at millimetre and submillimetre wavelengths. Both free–free and millimetre recombination line emission as star formation tracers have advantages over ultraviolet, optical, and near-infrared tracers in that they are unaffected by dust attenuation. Unlike infrared or radio continuum emission, the millimetre continuum and recombination line emission directly traces photoionized gas and therefore should be more reliable for measuring accurate star formation rates (SFRs). For additional discussion about this, see Murphy et al. (2011).

Millimetre continuum observations of nearby galaxies have been relatively straightforward, but the recombination line emission has been more difficult to detect. Before ALMA, millimetre recombination lines had been detected in multiple star-forming regions within the Milky Way (e.g. Waltman et al. 1973; Wilson & Pauls 1984; Gordon 1989; Gordon & Walmsley 1990), but extragalactic millimetre recombination line emission had only been detected in M82 (Seaquist, Kerton & Bell 1994; Seaquist et al. 1996), NGC 253 (Puxley et al. 1997), and Arp 220 (Anantharamaiah et al. 2000). ALMA is capable of reaching sensitivity levels at least an order of magnitude better than other telescopes (see Remijan, Adams & Warmels 2015, for a technical review) and can therefore lead to detections in many more nearby infrared-luminous sources than was previously possible (Scoville & Murchikova 2013). At this time, however, ALMA detections of specifically recombination line emission have been limited. Bendo et al. (2015b) and Meier et al. (2015) reported the detection of millimetre recombination line emission from the nearby starburst galaxy NGC 253, and Bendo et al. (2015b) used the 99.02 GHz continuum and H40α (99.02 GHz) line emission to

★E-mail: george.bendo@manchester.ac.uk

Keywords

The keywords are useful for indexing your paper's results.

Otherwise, the keywords are just a small formality in writing a paper.

Monthly Notices of the ROYAL ASTRONOMICAL SOCIETY

MNRAS 463, 252–269 (2016) doi:10.1093/mnras/stw1659
Advance Access publication 2016 July 11

Free–free and H42α emission from the dusty starburst within NGC 4945 as observed by ALMA

G. J. Bendo,[1,2]★ C. Henkel,[3,4] M. J. D'Cruze,[1] C. Dickinson,[1] G. A. Fuller[1,2] and A. Karim[5]

[1]*Jodrell Bank Centre for Astrophysics, School of Physics and Astronomy, The University of Manchester, Oxford Road, Manchester M13 9PL, UK*
[2]*UK ALMA Regional Centre Node*
[3]*Max-Planck-Institut für Radioastronomie, Auf dem Hügel 69, D-53121 Bonn, Germany*
[4]*Faculty of Science, Astronomy Department, King Abdulaziz University, PO Box 80203, Jeddah 21589, Saudi Arabia*
[5]*Argelander-Institut für Astronomie, Universität Bonn, Auf dem Hügel 71, D-53121 Bonn, Germany*

Accepted 2016 July 7. Received 2016 July 5; in original form 2016 April 7

ABSTRACT

We present observations of the 85.69 GHz continuum emission and H42α line emission from the central 30 arcsec within NGC 4945. Both sources of emission originate from nearly identical structures that can be modelled as exponential discs with scalelengths of ~2.1 arcsec (or ~40 pc). An analysis of the spectral energy distribution based on combining these data with archival data imply that 84 ± 10 per cent of the 85.69 GHz continuum emission originates from free–free emission. The electron temperature is 5400 ± 600 K, which is comparable to what has been measured near the centre of the Milky Way Galaxy. The star formation rate (SFR) based on the H42α and 85.69 GHz free–free emission (and using a distance of 3.8 Mpc) is 4.35 ± 0.25 $M_{\odot}$ yr^{-1}. This is consistent with the SFR from the total infrared flux and with previous measurements based on recombination line emission, and it is within a factor of ~2 of SFRs derived from radio data. The *Spitzer Space Telescope* 24 μm data and *Wide-field Infrared Survey Explorer* 22 μm data yield SFRs ~10× lower than the Atacama Large Millimeter/submillimeter Array measurements, most likely because the mid-infrared data are strongly affected by dust attenuation equivalent to A_V = 150. These results indicate that SFRs

Key words: galaxies: individual: NGC 4945 – galaxies: starburst – infrared: galaxies – radio continuum: galaxies – radio lines: galaxies.

1 INTRODUCTION

The Atacama Large Millimeter/submillimeter Array (ALMA) is capable of detecting two different forms of emission from photoionized gas in the star-forming regions within other galaxies. First, ALMA can measure continuum emission at 85–100 GHz where the spectral energy distributions (SEDs) of galaxies are dominated by free–free emission (e.g. Peel et al. 2011). Second, ALMA is sensitive enough to detect recombination line emission that appears at millimetre and submillimetre wavelengths. Both free–free and millimetre recombination line emission as star formation tracers have advantages over ultraviolet, optical, and near-infrared tracers in that they are unaffected by dust attenuation. Unlike infrared or radio continuum emission, the millimetre continuum and recombination line emission directly traces photoionized gas and therefore should be more reliable for measuring accurate star formation rates (SFRs). For additional discussion about this, see Murphy et al. (2011).

Millimetre continuum observations of nearby galaxies have been relatively straightforward, but the recombination line emission has been more difficult to detect. Before ALMA, millimetre recombination lines had been detected in multiple star-forming regions within the Milky Way (e.g. Waltman et al. 1973; Wilson & Pauls 1984; Gordon 1989; Gordon & Walmsley 1990), but extragalactic millimetre recombination line emission had only been detected in M82 (Seaquist, Kerton & Bell 1994; Seaquist et al. 1996), NGC 253 (Puxley et al. 1997), and Arp 220 (Anantharamaiah et al. 2000). ALMA is capable of reaching sensitivity levels at least an order of magnitude better than other telescopes (see Remijan, Adams & Warmels 2015, for a technical review) and can therefore lead to detections in many more nearby infrared-luminous sources than was previously possible (Scoville & Murchikova 2013). At this time, however, ALMA detections of specifically recombination line emission have been limited. Bendo et al. (2015b) and Meier et al. (2015) reported the detection of millimetre recombination line emission from the nearby starburst galaxy NGC 253, and Bendo et al. (2015b) used the 99.02 GHz continuum and H40α (99.02 GHz) line emission to

★E-mail: george.bendo@manchester.ac.uk

Introduction

The introduction serves three main purposes:

- It reviews the research material in the field.
- It explains why the research in the paper is needed.
- It explains what research is actually going to be presented in the paper.

Monthly Notices of the ROYAL ASTRONOMICAL SOCIETY

MNRAS **463**, 252–269 (2016) doi:10.1093/mnras/stw1659

Advance Access publication 2016 July 11

Free–free and H42α emission from the dusty starburst within NGC 4945 as observed by ALMA

G. J. Bendo,[1,2★] C. Henkel,[3,4] M. J. D'Cruze,[1] C. Dickinson,[1] G. A. Fuller[1,2] and A. Karim[5]

[1]*Jodrell Bank Centre for Astrophysics, School of Physics and Astronomy, The University of Manchester, Oxford Road, Manchester M13 9PL, UK*

[2]*UK ALMA Regional Centre Node*

[3]*Max-Planck-Institut für Radioastronomie, Auf dem Hügel 69, D-53121 Bonn, Germany*

[4]*Faculty of Science, Astronomy Department, King Abdulaziz University, PO Box 80203, Jeddah 21589, Saudi Arabia*

[5]*Argelander-Institut für Astronomie, Universität Bonn, Auf dem Hügel 71, D-53121 Bonn, Germany*

Accepted 2016 July 7. Received 2016 July 5; in original form 2016 April 7

ABSTRACT

We present observations of the 85.69 GHz continuum emission and H42α line emission from the central 30 arcsec within NGC 4945. Both sources of emission originate from nearly identical structures that can be modelled as exponential discs with scalelengths of ~2.1 arcsec (or ~40 pc). An analysis of the spectral energy distribution based on combining these data with archival data imply that 84 ± 10 per cent of the 85.69 GHz continuum emission originates from free–free emission. The electron temperature is 5400 ± 600 K, which is comparable to what has been measured near the centre of the Milky Way Galaxy. The star formation rate (SFR) based on the H42α and 85.69 GHz free–free emission (and using a distance of 3.8 Mpc) is 4.35 ± 0.25 $M_{\odot}$ yr^{-1}. This is consistent with the SFR from the total infrared flux and with previous measurements based on recombination line emission, and it is within a factor of ~2 of SFRs derived from radio data. The *Spitzer Space Telescope* 24 μm data and *Wide-field Infrared Survey Explorer* 22 μm data yield SFRs ~10× lower than the Atacama Large Millimeter/submillimeter Array measurements, most likely because the mid-infrared data are strongly affected by dust attenuation equivalent to $A_V = 150$. These results indicate that SFRs based on mid-infrared emission may be highly inaccurate for dusty, compact circumnuclear starbursts.

Key words: galaxies: individual: NGC 4945 – galaxies: starburst – infrared: galaxies – radio continuum: galaxies – radio lines: galaxies.

1 INTRODUCTION

The Atacama Large Millimeter/submillimeter Array (ALMA) is capable of detecting two different forms of emission from photoionized gas in the star-forming regions within other galaxies. First, ALMA can measure continuum emission at 85–100 GHz where the spectral energy distributions (SEDs) of galaxies are dominated by free–free emission (e.g. Peel et al. 2011). Second, ALMA is sensitive enough to detect recombination line emission that appears at millimetre and submillimetre wavelengths. Both free–free and millimetre recombination line emission as star formation tracers have advantages over ultraviolet, optical, and near-infrared tracers in that they are unaffected by dust attenuation. Unlike infrared or radio continuum emission, the millimetre continuum and recombination line emission directly traces photoionized gas and therefore should be more reliable for measuring accurate star formation rates (SFRs). For additional discussion about this, see Murphy et al. (2011).

Millimetre continuum observations of nearby galaxies have been relatively straightforward, but the recombination line emission has been more difficult to detect. Before ALMA, millimetre recombination lines had been detected in multiple star-forming regions within the Milky Way (e.g. Waltman et al. 1973; Wilson & Pauls 1984; Gordon 1989; Gordon & Walmsley 1990), but extragalactic millimetre recombination line emission had only been detected in M82 (Seaquist, Kerton & Bell 1994; Seaquist et al. 1996), NGC 253 (Puxley et al. 1997), and Arp 220 (Anantharamaiah et al. 2000). ALMA is capable of reaching sensitivity levels at least an order of magnitude better than other telescopes (see Remijan, Adams & Warmels 2015, for a technical review) and can therefore lead to detections in many more nearby infrared-luminous sources than was previously possible (Scoville & Murchikova 2013). At this time, however, ALMA detections of specifically recombination line emission have been limited. Bendo et al. (2015b) and Meier et al. (2015) reported the detection of millimetre recombination line emission from the nearby starburst galaxy NGC 253, and Bendo et al. (2015b) used the 99.02 GHz continuum and H40α (99.02 GHz) line emission to

★E-mail: george.bendo@manchester.ac.uk

Published by Oxford University Press on behalf of the Royal Astronomical Society

Data

The data section describes the data used in the analysis.

Since a lot of data is made public these days, it is very important to provide details on the data processing when possible so that people can replicate your results.

When reading a paper, though, the observations and data reduction can be rather uninteresting (unless you are trying to recreate someone else's images or spectra).

the future work on extragalactic star formation in nearby galaxies that can be done with ALMA.

2 DATA

The data were originally acquired as part of programme 2011.0.00172.S and published by Bolatto et al. (2013). The observations covering the H40α line are from three execution blocks (EBs) performed on 2012 May 07, July 01, and July 02. Three locations along the major axis spaced by 25 arcsec were observed, and the total integration time per location was 29 min. Only 14–20 antennas were operational. The spectral window covering the H40α line was centred at a sky frequency of 98.54 GHz, contained 3840 channels each with a width of 488 kHz (1.5 km s^{-1}), and included both polarizations. Uranus was the flux calibrator, J2333−237 was the bandpass calibrator, and J0137−245 was the phase calibrator.

We reprocessed the data using the Common Astronomy Software Applications version 4.2.2, which includes a version of the flux calibration (Butler-JPL-Horizons 2012) that is more up to date than the one used to create the data in the ALMA archive. The visibility data were processed through steps to flag bad data and to calibrate the phase and amplitude as a function of frequency and time. Next, we rescaled the amplitudes of the visibility data so that the signal measured for J0137−245 in the individual EBs matched the weighted average of these values, and then we concatenated the data. We produced two versions of the image cube (with and without continuum) using a clean algorithm with natural weightings in an interactive mode. Although the primary beam is 63 arcsec, we created image cubes covering a 32 × 32 arcsec region (with 0.1 arcsec pixels) because no detectable emission is found outside this region. The cubes used in the analysis cover a sky frequency range between 98.80 and 99.09 GHz, and each channel in each cube covers eight channels in the visibility data, which corresponds to 3.9 MHz (~11.8 km s^{-1}). For display purposes, we also produced a cube that covered 97.64–99.44 GHz, which was the full usable range of the spectral window containing the H40α line, with the same spatial and spectral resolution. The full width at half-maximum (FWHM) of the reconstructed beam is 1.9 × 1.6 arcsec; assuming a distance of 3.44 ± 0.26 Mpc (based on the average of distances measured by Dalcanton et al. 2009), this corresponds to spatial scales of ~30 pc. The flux calibration uncertainty reported in the ALMA Technical Handbook is 5 per cent (Lundgren 2013). The 98.54 GHz flux densities for the bandpass calibrator (1.15 ± 0.04 Jy) and the phase calibrator (1.09 ± 0.06 Jy) have relative uncertainties (based on the variations in measurements from individual EBs) that are consistent with the Technical Handbook, although unidentified systematic amplitude calibration effects could affect the flux densities. Cleaned image cubes of the bandpass and phase calibrators show <1 per cent variations in the flux density from channel to channel, and no spectral features are seen at the position of the H40α line in the visibility data for the calibration sources, which indicates that any line emission >1 per cent of the continuum emission is not caused by calibration issues.

We had access to data from programme 2011.0.00061.S (PI: Takano) that also covers the H40α line. Because the spectral settings were different from programme 2011.0.00172.S, we did not use the data in our analysis, but we did examine the processed archival data for programme 2011.0.00061.S to confirm that the H40α emission is detected in those data.

H40α fluxes, mean velocities (relative to the Solar system barycentre), and velocity FWHM were measured in the continuum-subtracted image cube, and the continuum at 99.02 GHz was measured in the other image cube by fitting and removing the line emission. Images of the continuum emission (based on all continuum data within the spectral window), the H40α flux, and the H40α mean velocity are shown in Fig. 1. Spectra integrated over the central 20 × 10 arcsec as well as integrated within regions covering the three brightest regions are shown in Fig. 2. Details of the measurements in these regions are listed in Table 1. The uncertainties in the measurements incorporate the noise per channel values listed in Table 1, but except for the east (E) region, the accuracy in the continuum and H40α fluxes is primarily limited by the calibration uncertainties. Most of the signal outside the 20 × 10 arcsec ellipse is detected at $\lesssim 3\sigma$, and we also lack the uv coverage to recover >20 arcsec structures.

The central star-forming region can be divided into three knots that lie along the major axis of the galaxy. The central (C) and west (W) sources are detected at $>10\sigma$ in both the continuum and H40α emission. The eastern source is detected at $>10\sigma$ in continuum emission as well, but the peak is only detected at the $\sim 8\sigma$ level in H40α emission. Although all three sources had previously been detected in radio continuum emission (Mohan et al. 2005; Kepley et al. 2011), only Anantharamaiah & Goss (1996) had previously shown radio recombination line emission from all three sources.

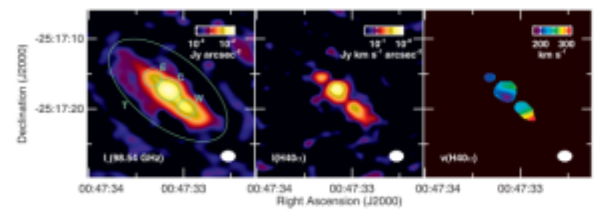

Figure 1. Images of the continuum surface brightness, the H40α intensity, and the H40α mean velocity in the central 32 × 32 arcsec of NGC 253. The velocity, which is relative to the Solar system barycentre, is only shown for data where the H40α intensity is detected at the 5σ level. The white oval at the bottom right of each panel shows the FWHM of the beam. The green regions in the continuum image show the total (T), east (E), central (C), and west (W) regions within which fluxes and spectra were measured. The spectra are shown in Fig. 2, and measured quantities are listed in Table 1.

The data section could often be split into a few different sections, such as the following:

- **Sample** – People often select subsets of objects to work with and need to explain how they selected these objects.
- **Observations** – If the paper is presenting new data, it is important to describe how those observations were done.
- **Data reduction** – It is important to document how the observations were converted into actual usable images or spectra.

Dust heating mechanisms in nearby galaxies 137

because the dust is heated by young stars but instead because the dust traces the gas fuelling star formation, as suggested by Boquien et al. (2011) and Bendo et al. (2012a). If so, then this could affect how star formation is calculated using far-infrared flux measurements and could also affect the analyses of things such as gas-depletion times in normal and starburst galaxies, the far-infrared-to-radio correlation, and the 'main-sequence' relation between star formation rate and stellar mass.

To better understand dust heating mechanisms within nearby galaxies, we present here an expanded comparison of infrared surface brightness ratios to dust heating sources within a set of 24 face-on spiral galaxies with well-resolved far-infrared emission that consists of 11 galaxies from the HRS, 10 galaxies from the Key Insights on Nearby Galaxies: A Far-Infrared Survey with *Herschel* (KINGFISH; Kennicutt et al. 2011), and the three galaxies from Bendo et al. (2012a). This larger sample of galaxies can be used to determine whether the cold dust component heated by the evolved stellar population is consistently seen among all spiral galaxies or if, in some spiral galaxies, star formation may be the dominant heating source for the dust seen at all wavelengths. Additionally, with the larger sample of galaxies, it will be possible to look at variations in the relative contributions of star-forming regions and the evolved stellar populations among a large sample of galaxies [as already seen within the three galaxies studied by Bendo et al. (2012a)] and to possibly link these variations with other physical properties of the galaxies.

The analysis primarily focuses on the 160/250 and 250/350 μm surface brightness ratios based on 160 μm data taken with the Photodetector Array Camera and Spectrometer (PACS; Poglitsch et al. 2010) and 250 and 350 μm data taken with the Spectral and Photometric Imaging REceiver (SPIRE; Griffin et al. 2010). These data cover the transition between warmer dust heated by star-forming regions and colder dust heated by the evolved stellar population found previously by Bendo et al. (2010, 2012a) and Boquien et al. (2011), so this is a good part of the far-infrared waveband to examine. We had PACS 70 and 100 μm data for most galaxies in our sample but did not use it in most of our analysis because we had difficulty detecting emission above a 3σ threshold from diffuse low surface brightness regions, particularly in the outer parts of the optical discs. SPIRE 500 μm data were also available, but we did not use the data mainly because the 500 μm point spread function (PSF) has a full width at half-maximum (FWHM) of 36 arcsec, which would cause problems with attempting to resolve structures within many of the sample galaxies. Moreover, although Bendo et al. (2012a) was still able to relate the 350/500 μm variations in their galaxies to heating sources, it was clear that the 350/500 μm ratios were relatively insensitive to temperature variations compared to shorter wavelength ratios. For these reasons, we limit our analyses to the 160/250 and 250/350 μm ratios.

Following descriptions of the sample in Section 2 and the data in Section 3, we present three different parts of the analysis. Section 4 presents a qualitative analysis in which we compare 160/250 and 250/350 μm surface brightness ratio maps to tracers of star-forming regions and the evolved stellar population. Section 5 presents a quantitative comparison of the 160/250 and 250/350 μm ratios to the tracers of these two different heating sources. Section 6 includes an analytical approach first proposed by Bendo et al. (2012a) in which the 160/250 and 250/350 μm ratios are fitted as a function of both the evolved stellar population and star formation; the results of the fits can be used to determine the fraction of the variation in the surface brightness ratios that can be attributed to a dust heating source. After this analysis, we discuss the implications of the results for modelling dust emission and for measuring star formation rates in Section 7. A summary of our results for each galaxy as well as for the sample as a whole is presented in Section 8.

2 SAMPLE

As stated in the introduction, the sample used for this analysis is drawn from three other samples: HRS, KINGFISH, and the Bendo et al. (2012a) sample, which is a subsample of galaxies from the Very Nearby Galaxies Survey (VNGS; PI: C. Wilson). The three surveys have different purposes. The HRS is a complete sample of 323 galaxies that fall within distances between 15 and 25 Mpc that are also brighter than *K*-band total magnitude of 12 (applied to Sa-Im and blue compact dwarf galaxies) or 8.7 (applied to E, S0, and S0a galaxies). This survey is intended to provide statistical information about the properties of galaxies (*e.g.* far-infrared colours, far-infrared luminosities, dust temperatures, dust masses, dust emissivities, etc.). KINGFISH is a continuation of the *Spitzer* Infrared Nearby Galaxies Survey (SINGS; Kennicutt et al. 2003) and consists of a sample of galaxies selected to span a range of morphologies, infrared luminosities, and infrared/optical luminosity ratios. The sample does not have the same applications as a volume- or flux-limited sample, but since SINGS and KINGFISH have also gathered additional infrared spectral data and other ancillary data for the galaxies, the sample is very useful for multiwavelength analyses. The VNGS is a project that observed 13 galaxies with *Herschel*, and while the sample is not a statistically complete or representative sample, it includes many very well-studied nearby galaxies, many of which are archetypal representatives of a class of objects (*e.g.* Arp 220, Cen A, M82).

Using data from all three of these surveys is not ideal, as the resulting sample is somewhat heterogeneous. However, given the stringent selection criteria that we needed to apply, it was necessary to select galaxies from multiple surveys to build up our sample. The HRS and KINGFISH samples were used mainly because they are two of the largest photometric surveys performed with *Herschel* that included spiral galaxies. The VNGS galaxies were included mainly because the data from the previous analysis are already in hand.

To select galaxies for our analysis, we applied the following criteria.

(1) The galaxies must have morphological types between Sa and Sd. Irregular galaxies have low infrared surface brightnesses, making it difficult for us to apply our analysis methods. Emission from E-S0/a galaxies is generally compact (e.g. Bendo et al. 2007; Muñoz-Mateos et al. 2009; Smith et al. 2012a), so the infrared emission observed by *Herschel* is usually unresolved or marginally resolved, and our analysis will not work. In the cases where emission is detected in extended structures in E-S0/a galaxies (such as NGC 1291 or NGC 4406), it is impractical to work with the data because of the relatively low surface brightness of the extended emission.

(2) The galaxies must be face-on (with minor/major axis ratios of >0.5). This eliminates edge-on and steeply inclined galaxies where integration along the line of sight may complicate the analysis.

(3) The galaxies must have optical major axes that are >5 arcmin. This ensures that sufficient data are available to examine substructures within the galaxies at the resolution of the 350 μm data.

(4) After the application of the data preparation steps in Section 3.4, the 250/350 μm surface brightness ratio must be measured at the 3σ level within a ≥7 arcmin^2 area (which is equivalent to the area of a circle with a diameter of ≥3 arcmin). This ensures

MNRAS 448, 135–167 (2015)

The data section could often be split into a few different sections, such as the following:

- **Sample** – People often select subsets of objects to work with and need to explain how they selected these objects.
- **Observations** – If the paper is presenting new data, it is important to describe how those observations were done.
- **Data reduction** – It is important to document how the observations were converted into actual usable images or spectra.

SPITZER AND JCMT OBS

only with the limited resolution of previous instrumentation. The major problem is that many nearby Seyfert galaxies have circumnuclear star formation that will produce centralized dust emission that is difficult to disentangle from far-infrared emission from dust heated by the AGN. Both sources of emission are effectively superimposed.

The Sombrero Galaxy (NGC 4954), at a distance of 9.2 Mpc (the average of measurements from Ford et al. 1996 and Ajhar et al. 1997), is ideal for studying the separate SEDs of dust heated by the AGN and dust heated by starlight. The galaxy's nucleus is classified in Ho et al. (1997) as a low-ionization nuclear emission region (LINER). It does contain a supermassive black hole with a mass of $10^9\ M_\odot$ (Kormendy et al. 1996), and the AGN is detected as a point source in hard X-ray (e.g., Pellegrini et al. 2002, 2003) and radio (e.g., Hummel et al. 1984) emission. What makes this particular LINER unique is that the geometry of the mid- and far-infrared dust emission is relatively easy to model, and the dust that is primarily heated by star formation is mostly concentrated in a ring relatively far from the AGN, as we demonstrate in this paper. Therefore, the SED of the dust heated by the AGN can be separated from the SED of the diffuse interstellar dust. This galaxy has been studied in the infrared/submillimeter wave band in previous works (e.g., Rice et al. 1988; Schmitt et al. 1997; Krause et al. 2006), but these studies were limited by the resolution of the *IRAS* data and could only examine the global SED in the far-infrared.

In this paper we present *Spitzer Space Telescope* (Werner et al. 2004) Infrared Array Camera (IRAC; Fazio et al. 2004) 3.6–8.0 μm images, Multiband Imaging Photometer for *Spitzer* (MIPS; Rieke et al. 2004) 24–160 μm images, and Infrared Spectrograph (IRS; Houck et al. 2004) mid-infrared spectra, as well as James Clerk Maxwell Telescope (JCMT) Submillimeter Common-User Bolometer Array (SCUBA; Holland et al. 1999) 850 μm images of the Sombrero Galaxy that we use to examine the separate SEDs of the AGN and the dust ring. In § 2 we describe the observations and data reductions. In § 3.1 we discuss the images qualitatively. In § 3.2 we briefly discuss the IRS mid-infrared spectra. In § 3.3 we model the images of the galaxy in each wave band to determine SEDs for global emission and for the separate physical com-

2. OBSERVATIONS AND DATA REDUCTION

2.1. 3.6–8.0 μm *Images*

The 3.6–8.0 μm data were taken with IRAC on the *Spitzer Space Telescope* on 2004 June 10 in IRAC campaign 9 and on 2005 January 22 in IRAC campaign 18 as part of the *Spitzer* Infrared Nearby Galaxies Survey (SINGS; Kennicutt et al. 2003). The observations consist of a series of $5' \times 5'$ individual frames that are offset 2.'5 from each other. The two separate sets of observations allow asteroids to be recognized and provide observations at orientations up to a few degrees apart to ease removal of detector artifacts. Points in the center are imaged 8 times in 30 s exposures. The FWHM of the point-spread functions (PSFs) are 1.'6–1.'9 for the four wave bands.

The data are processed using a special SINGS IRAC pipeline. First, a geometric distortion correction is applied to the individual frames. Data from the second set of observations are rotated to the same orientation as the first set of observations. Bias levels are subtracted from the 5.7 μm data by subtracting a bias frame (made by combining all data frames for the observations) from each frame. Next, the image offsets are determined through image cross-correlation. Following this, bias drift is removed. Finally, cosmic-ray masks are created using standard drizzle methods, and final image mosaics are created using a drizzle technique. The final pixel scales are set at ~0.''75. A final background is measured in small regions outside the target that are free of bright foreground/background sources, and then this final background is subtracted from the data. The contribution of uncertainties in the background (both in terms of the statistical fluctuations of the pixels and the uncertainty in the mean background subtracted from the data) to uncertainties in the integrated global flux densities is less than 0.1%. The dominant source of uncertainty is the 30% uncertainty in the calibration factor (including the uncertainty in the extended source calibration) applied to the final mosaics.

2.2. 24–160 μm *Images*

The 24, 70, and 160 μm data were taken with MIPS on the *Spitzer Space Telescope* on 2004 July 10 and 12 in MIPS campaign 10 as part of the SINGS survey. The observations were obtained using the scan-mapping mode in two separate visits to the galaxy. Two separate sets of observations separated by more than 24 hr allow asteroids to be recognized and provide observations at orientations up to a few degrees apart to ease removal of detector artifacts. As a result of redundancy inherent in the scan-mapping mode, each pixel in the core map area was effectively observed 40, 20, and 4 times at 24, 70, and 160 μm, respectively, resulting in integration times per pixel of 160, 80, and 16 s, respectively. The FWHM of the PSFs of the 24, 70, and 160 μm data are 6'', 15'', and 40'', respectively.

The MIPS data were processed using the MIPS Data Analysis Tools version 2.80 (Gordon et al. 2005). The processing for the 24 μm data differed notably from the 70 and 160 μm data, so they are discussed separately.

First, the 24 μm images were processed through a droop correction (that removes an excess signal in each pixel that is proportional to the signal in the entire array) and a nonlinearity correction. Following this, the dark current was subtracted. Next, scan-mirror-position–dependent flats and scan-mirror-position–independent flats were applied to the data. Latent images from bright sources, erroneously high or low pixel values, and unusually noisy frames were also masked out. Finally, mosaics of the data from each set of observations were made. In each mosaic, the background was subtracted in two steps. First, to remove the broad zodiacal light emission, a function that varied linearly in the *x*- and *y*-directions was fit to the region outside the optical disk in a box 3 times the size of the optical major axis of the galaxy. This plane was then subtracted from the data. Next, to remove residual background emission from cirrus structure near the galaxy, an additional offset measured in multiple small circular regions near the optical disk was subtracted. After this final subtraction, the two mosaics were averaged together to produce the final 24 μm mosaic.

In the 70 and 160 μm data, readout jumps and cosmic-ray hits were first removed from the data. Next, the stim flash frames taken by the instrument were used as responsivity corrections. The dark current was subtracted from the data, an illumination correction was applied, and then short-term variations in signal (i.e., short-term drift) were subtracted from the data. (This last step also subtracts off the background.) Following this, erroneously high or low pixel values were identified statistically or visually and removed from the data. Single 70 and 160 μm mosaics were made from all of the data, and a residual offset measured in two regions to the north and south of the target was subtracted from the final maps.

The background noise is a relatively small contributor (less than 0.1%) to the uncertainties in the integrated global flux densities. The dominant source of uncertainty is the uncertainty in

Analysis

The analysis contains the science results presented by the paper.

However, the paper may examine multiple science questions, in which case the analysis may actually be divided across multiple sections.

This part of the paper also usually has the most important images.

Figure 4. The original 250 μm image of M81 (top), the 250 μm image afte[r] it has been convolved with a kernel to match the PSF to that of the 500 μ[m] data (middle) and the convolved 250 μm image after rebinning (bottom[)]. The green circles show the FWHM of the PSF of the data. In the convolve[d] ...

4 ANALYSIS

4.1 Colour temperature maps

Figs 5–7 show the colour temperatures based on the surface brightness ratios produced by this analysis. The colour temperatures are calculated using

$$\frac{I_\nu(\lambda_1)}{I_\nu(\lambda_2)} = \left(\frac{\lambda_2}{\lambda_1}\right)^{3+\beta} \left(\frac{e^{hc/\lambda_2 kT} - 1}{e^{hc/\lambda_1 kT} - 1}\right) \quad (5)$$

in which dust emission is treated as originating from a single component that is optically thin in the far-infrared. The parameter β is the dust emissivity coefficient that indicates how the emissivity scales as a function of wavelength. We use $\beta = 2$ (given by Li & Draine 2001) for this calculation, as it has previously been shown to accurately describe the observed emissivity of dust. The colour temperature maps for each galaxy look notably different in comparison to the stellar and dust structures in Figs 1–3. The emission in some bands, particularly the shorter wavelength ones, may originate from dust with a range of temperatures. Moreover, temperatures determined from the Rayleigh–Jeans side of the SED may be improperly constrained without using data from the Wien side of the peak. Hence, these colour temperatures should be used to aid in relating the colour variations in the maps to the SED shape and should not necessarily be interpreted as the physical dust temperatures, even though this could be the case for the colour temperatures based on the longer wavelength bands. Also, the 350/500 μm colour temperatures tend to appear noisier. Both wavebands sample locations on the Rayleigh–Jeans tail of the dust SED and are therefore relatively less sensitive to temperature variations, which causes the images to appear noisy.

The M81 colour temperature maps are simply modified versions of the ratio maps published by Bendo et al. (2010b). The 70/160 μm colour temperatures and, to a limited degree, the 160/250 μm colour temperatures are enhanced in the spiral arms. However, the 160/250 μm, 250/350 μm and 350/500 μm colour temperature maps appear to be dominated by radial variations in the colour temperatures. This implies that the colour variations between 160 and 500 μm are dependent either on galactocentric radius or on stellar surface brightness.

The M83 colour temperature maps show enhancements near the nucleus and along spiral arms near star-forming regions. The structures in the 70/160 μm and 160/250 μm colour temperature maps clearly trace Hα regions along the edges of the spiral arms instead of the stellar structures seen in the 1.6 μm image, suggesting that these colour temperatures are linked to the star formation activity. We observe these structures on the leading edges of both spiral arms, which demonstrates that the structures are not simply the result of a misalignment in astrometry between two pairs of images. The relatively smooth gradient in the 250/350 μm colour temperature is consistent with the gradient in the 1.6 μm maps, and the central region with 250/350 μm colour temperatures above 30 K, while very noisy, appears to correspond roughly to the bar seen in the 1.6 μm image. This suggests that the 250/350 μm colour temperatures could be affected by heating by the total stellar population. Foyle et al. (in preparation) are performing an analysis that more carefully examines the colour gradients across the arms and the bar. While the nucleus itself appears to have enhanced 70/160 μm colour temperatures, the regions with the most strongly enhanced colour temperatures in the other bands are the regions just to the east and west of the nucleus. The reason for this is unclear. One possibility is that the PSF matching is imperfect and residual side lobes have appeared around the very bright nucleus in some of the data. However, such artefacts are not seen for other sources processed in the same way (see e.g. VS 44 in NGC 2403). Another possibility is that some of the dust in the nucleus itself is relatively cold because the dust shields itself from the nuclear starburst, but the regions immediately outside the nucleus are not as well shielded and thus become warmer in all wavebands. The nuclear colour temperature structure is poorly resolved in the resolutions that we are working at and the structures are relatively sensitive to 1–2 arcsec adjustments in astrometry (although the binned data are unaffected by such adjustments), so it is difficult to accurately assess this with the data in hand. Future work with higher-resolution data is warranted.

The NGC 2403 colour temperature maps show significant differences in the dust heating between 70 and 500 μm. The 70/160 μm colour temperature map shows temperature enhancements mainly at locations with bright star-forming regions. However, these regions

Discussion

The discussion section usually states the implications for the analysis results.

This is also a good place to discuss the analysis results from your paper in the context of results from other papers.

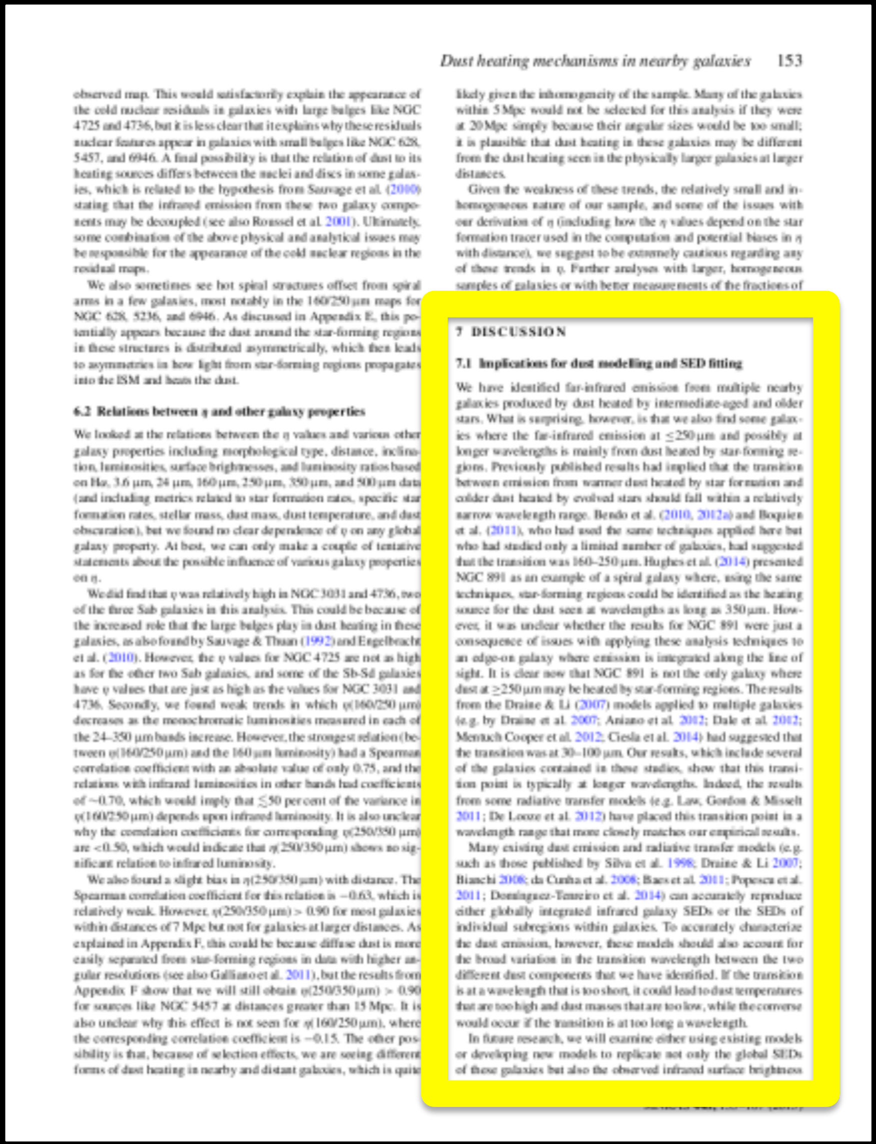

observed map. This would satisfactorily explain the appearance of the cold nuclear residuals in galaxies with large bulges like NGC 4725 and 4736, but it is less clear that it explains why these residuals nuclear features appear in galaxies with small bulges like NGC 628, 5457, and 6946. A final possibility is that the relation of dust to its heating sources differs between the nuclei and discs in some galaxies, which is related to the hypothesis from Sauvage et al. (2010) stating that the infrared emission from these two galaxy components may be decoupled (see also Roussel et al. 2001). Ultimately, some combination of the above physical and analytical issues may be responsible for the appearance of the cold nuclear regions in the residual maps.

We also sometimes see hot spiral structures offset from spiral arms in a few galaxies, most notably in the 160/250 μm maps for NGC 628, 5236, and 6946. As discussed in Appendix E, this potentially appears because the dust around the star-forming regions in these structures is distributed asymmetrically, which then leads to asymmetries in how light from star-forming regions propagates into the ISM and heats the dust.

6.2 Relations between η and other galaxy properties

We looked at the relations between the η values and various other galaxy properties including morphological type, distance, inclination, luminosities, surface brightnesses, and luminosity ratios based on Hα, 3.6 μm, 24 μm, 160 μm, 250 μm, 350 μm, and 500 μm data (and including metrics related to star formation rates, specific star formation rates, stellar mass, dust mass, dust temperature, and dust obscuration), but we found no clear dependence of η on any global galaxy property. At best, we can only make a couple of tentative statements about the possible influence of various galaxy properties on η.

We did find that η was relatively high in NGC 3031 and 4736, two of the three Sab galaxies in this analysis. This could be because of the increased role that the large bulges play in dust heating in these galaxies, as also found by Sauvage & Thuan (1992) and Engelbracht et al. (2010). However, the η values for NGC 4725 are not as high as for the other two Sab galaxies, and some of the Sb-Sd galaxies have η values that are just as high as the values for NGC 3031 and 4736. Secondly, we found weak trends in which η(160/250 μm) decreases as the monochromatic luminosities measured in each of the 24–350 μm bands increase. However, the strongest relation (between η(160/250 μm) and the 160 μm luminosity) had a Spearman correlation coefficient with an absolute value of only 0.75, and the relations with infrared luminosities in other bands had coefficients of ~0.70, which would imply that $\lesssim$50 per cent of the variance in η(160/250 μm) depends upon infrared luminosity. It is also unclear why the correlation coefficients for corresponding η(250/350 μm) are <0.50, which would indicate that η(250/350 μm) shows no significant relation to infrared luminosity.

We also found a slight bias in η(250/350 μm) with distance. The Spearman correlation coefficient for this relation is −0.63, which is relatively weak. However, η(250/350 μm) > 0.90 for most galaxies within distances of 7 Mpc but not for galaxies at larger distances. As explained in Appendix F, this could be because diffuse dust is more easily separated from star-forming regions in data with higher angular resolutions (see also Galliano et al. 2011), but the results from Appendix F show that we will still obtain η(250/350 μm) > 0.90 for sources like NGC 5457 at distances greater than 15 Mpc. It is also unclear why this effect is not seen for η(160/250 μm), where the corresponding correlation coefficient is −0.15. The other possibility is that, because of selection effects, we are seeing different forms of dust heating in nearby and distant galaxies, which is quite likely given the inhomogeneity of the sample. Many of the galaxies within 5 Mpc would not be selected for this analysis if they were at 20 Mpc simply because their angular sizes would be too small; it is plausible that dust heating in these galaxies may be different from the dust heating seen in the physically larger galaxies at larger distances.

Given the weakness of these trends, the relatively small and inhomogeneous nature of our sample, and some of the issues with our derivation of η (including how the η values depend on the star formation tracer used in the computation and potential biases in η with distance), we suggest to be extremely cautious regarding any of these trends in η. Further analyses with larger, homogeneous samples of galaxies or with better measurements of the fractions of

7 DISCUSSION

7.1 Implications for dust modelling and SED fitting

We have identified far-infrared emission from multiple nearby galaxies produced by dust heated by intermediate-aged and older stars. What is surprising, however, is that we also find some galaxies where the far-infrared emission at $\lesssim$250 μm and possibly at longer wavelengths is mainly from dust heated by star-forming regions. Previously published results had implied that the transition between emission from warmer dust heated by star formation and colder dust heated by evolved stars should fall within a relatively narrow wavelength range. Bendo et al. (2010, 2012a) and Boquien et al. (2011), who had used the same techniques applied here but who had studied only a limited number of galaxies, had suggested that the transition was 160–250 μm. Hughes et al. (2014) presented NGC 891 as an example of a spiral galaxy where, using the same techniques, star-forming regions could be identified as the heating source for the dust seen at wavelengths as long as 350 μm. However, it was unclear whether the results for NGC 891 were just a consequence of issues with applying these analysis techniques to an edge-on galaxy where emission is integrated along the line of sight. It is clear now that NGC 891 is not the only galaxy where dust at $\gtrsim$250 μm may be heated by star-forming regions. The results from the Draine & Li (2007) models applied to multiple galaxies (e.g. by Draine et al. 2007; Aniano et al. 2012; Dale et al. 2012; Mentuch Cooper et al. 2012; Ciesla et al. 2014) had suggested that the transition was at 30–100 μm. Our results, which include several of the galaxies contained in these studies, show that this transition point is typically at longer wavelengths. Indeed, the results from some radiative transfer models (e.g. Law, Gordon & Misselt 2011; De Looze et al. 2012) have placed this transition point in a wavelength range that more closely matches our empirical results.

Many existing dust emission and radiative transfer models (e.g. such as those published by Silva et al. 1998; Draine & Li 2007; Bianchi 2008; da Cunha et al. 2008; Baes et al. 2011; Popescu et al. 2011; Dominguez-Tenreiro et al. 2014) can accurately reproduce either globally integrated infrared galaxy SEDs or the SEDs of individual subregions within galaxies. To accurately characterize the dust emission, however, these models should also account for the broad variation in the transition wavelength between the two different dust components that we have identified. If the transition is at a wavelength that is too short, it could lead to dust temperatures that are too high and dust masses that are too low, while the converse would occur if the transition is at too long a wavelength.

In future research, we will examine either using existing models or developing new models to replicate not only the global SEDs of those galaxies but also the observed infrared surface brightness

Conclusions

The conclusions should provide a quick summary of the important science results from the paper.

The conclusions do not need to summarize the entire paper.

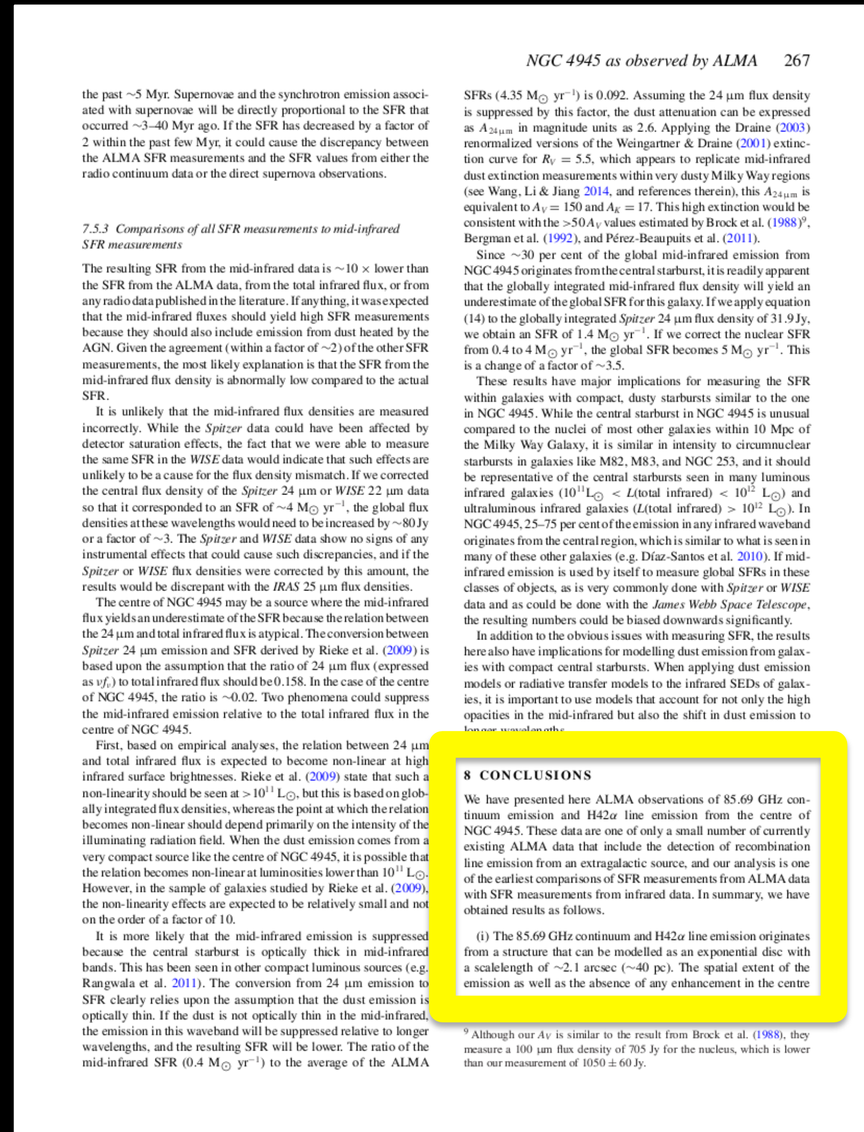

the past ∼5 Myr. Supernovae and the synchrotron emission associated with supernovae will be directly proportional to the SFR that occurred ∼3–40 Myr ago. If the SFR has decreased by a factor of 2 within the past few Myr, it could cause the discrepancy between the ALMA SFR measurements and the SFR values from either the radio continuum data or the direct supernova observations.

7.5.3 Comparisons of all SFR measurements to mid-infrared SFR measurements

The resulting SFR from the mid-infrared data is ∼10 × lower than the SFR from the ALMA data, from the total infrared flux, or from any radio data published in the literature. If anything, it was expected that the mid-infrared fluxes should yield high SFR measurements because they should also include emission from dust heated by the AGN. Given the agreement (within a factor of ∼2) of the other SFR measurements, the most likely explanation is that the SFR from the mid-infrared flux density is abnormally low compared to the actual SFR.

It is unlikely that the mid-infrared flux densities are measured incorrectly. While the *Spitzer* data could have been affected by detector saturation effects, the fact that we were able to measure the same SFR in the *WISE* data would indicate that such effects are unlikely to be a cause for the flux density mismatch. If we corrected the central flux density of the *Spitzer* 24 μm or *WISE* 22 μm data so that it corresponded to an SFR of ∼4 $M_\odot$ yr^{-1}, the global flux densities at these wavelengths would need to be increased by ∼80 Jy or a factor of ∼3. The *Spitzer* and *WISE* data show no signs of any instrumental effects that could cause such discrepancies, and if the *Spitzer* or *WISE* flux densities were corrected by this amount, the results would be discrepant with the *IRAS* 25 μm flux densities.

The centre of NGC 4945 may be a source where the mid-infrared flux yields an underestimate of the SFR because the relation between the 24 μm and total infrared flux is atypical. The conversion between *Spitzer* 24 μm emission and SFR derived by Rieke et al. (2009) is based upon the assumption that the ratio of 24 μm flux (expressed as νf_ν) to total infrared flux should be 0.158. In the case of the centre of NGC 4945, the ratio is ∼0.02. Two phenomena could suppress the mid-infrared emission relative to the total infrared flux in the centre of NGC 4945.

First, based on empirical analyses, the relation between 24 μm and total infrared flux is expected to become non-linear at high infrared surface brightnesses. Rieke et al. (2009) state that such a non-linearity should be seen at $>10^{11}$ $L_\odot$, but this is based on globally integrated flux densities, whereas the point at which the relation becomes non-linear should depend primarily on the intensity of the illuminating radiation field. When the dust emission comes from a very compact source like the centre of NGC 4945, it is possible that the relation becomes non-linear at luminosities lower than 10^{11} $L_\odot$. However, in the sample of galaxies studied by Rieke et al. (2009), the non-linearity effects are expected to be relatively small and not on the order of a factor of 10.

It is more likely that the mid-infrared emission is suppressed because the central starburst is optically thick in mid-infrared bands. This has been seen in other compact luminous sources (e.g. Rangwala et al. 2011). The conversion from 24 μm emission to SFR clearly relies upon the assumption that the dust emission is optically thin. If the dust is not optically thin in the mid-infrared, the emission in this waveband will be suppressed relative to longer wavelengths, and the resulting SFR will be lower. The ratio of the mid-infrared SFR (0.4 $M_\odot$ yr^{-1}) to the average of the ALMA SFRs (4.35 $M_\odot$ yr^{-1}) is 0.092. Assuming the 24 μm flux density is suppressed by this factor, the dust attenuation can be expressed as $A_{24\,\mu m}$ in magnitude units as 2.6. Applying the Draine (2003) renormalized versions of the Weingartner & Draine (2001) extinction curve for $R_V = 5.5$, which appears to replicate mid-infrared dust extinction measurements within very dusty Milky Way regions (see Wang, Li & Jiang 2014, and references therein), this $A_{24\,\mu m}$ is equivalent to $A_V = 150$ and $A_K = 17$. This high extinction would be consistent with the $>50 A_V$ values estimated by Brock et al. (1988)[9], Bergman et al. (1992), and Pérez-Beaupuits et al. (2011).

Since ∼30 per cent of the global mid-infrared emission from NGC 4945 originates from the central starburst, it is readily apparent that the globally integrated mid-infrared flux density will yield an underestimate of the global SFR for this galaxy. If we apply equation (14) to the globally integrated *Spitzer* 24 μm flux density of 31.9 Jy, we obtain an SFR of 1.4 $M_\odot$ yr^{-1}. If we correct the nuclear SFR from 0.4 to 4 $M_\odot$ yr^{-1}, the global SFR becomes 5 $M_\odot$ yr^{-1}. This is a change of a factor of ∼3.5.

These results have major implications for measuring the SFR within galaxies with compact, dusty starbursts similar to the one in NGC 4945. While the central starburst in NGC 4945 is unusual compared to the nuclei of most other galaxies within 10 Mpc of the Milky Way Galaxy, it is similar in intensity to circumnuclear starbursts in galaxies like M82, M83, and NGC 253, and it should be representative of the central starbursts seen in many luminous infrared galaxies ($10^{11} L_\odot < L(\text{total infrared}) < 10^{12}\ L_\odot$) and ultraluminous infrared galaxies ($L(\text{total infrared}) > 10^{12}\ L_\odot$). In NGC 4945, 25–75 per cent of the emission in any infrared waveband originates from the central region, which is similar to what is seen in many of these other galaxies (e.g. Díaz-Santos et al. 2010). If mid-infrared emission is used by itself to measure global SFRs in these classes of objects, as is very commonly done with *Spitzer* or *WISE* data and as could be done with the *James Webb Space Telescope*, the resulting numbers could be biased downwards significantly.

In addition to the obvious issues with measuring SFR, the results here also have implications for modelling dust emission from galaxies with compact central starbursts. When applying dust emission models or radiative transfer models to the infrared SEDs of galaxies, it is important to use models that account for not only the high opacities in the mid-infrared but also the shift in dust emission to longer wavelengths.

8 CONCLUSIONS

We have presented here ALMA observations of 85.69 GHz continuum emission and H42α line emission from the centre of NGC 4945. These data are one of only a small number of currently existing ALMA data that include the detection of recombination line emission from an extragalactic source, and our analysis is one of the earliest comparisons of SFR measurements from ALMA data with SFR measurements from infrared data. In summary, we have obtained results as follows.

(i) The 85.69 GHz continuum and H42α line emission originates from a structure that can be modelled as an exponential disc with a scalelength of ∼2.1 arcsec (∼40 pc). The spatial extent of the emission as well as the absence of any enhancement in the centre

[9] Although our A_V is similar to the result from Brock et al. (1988), they measure a 100 μm flux density of 705 Jy for the nucleus, which is lower than our measurement of 1050 ± 60 Jy.

Conclusions

The conclusions should provide a quick summary of the important science results from the paper.

The conclusions do not need to summarize the entire paper.

as well as the absence of any broad line emission suggest that the emission originates primarily from photoionized gas associated with the circumnuclear starburst and not from the AGN.

(ii) The SED for the central source implies that 84 ± 10 per cent of the 85.69 GHz continuum emission from the central disc originates from free–free emission.

(iii) The T_e for the central star-forming disc based on the ratio of the H42α line emission to 85.69 GHz free–free emission is 5400 ± 600 K. This is similar to what is measured near the centre of the Milky Way. These results also imply that the AGN contributes ≲10 per cent of the total continuum emission from the central disc.

(iv) The SFR for the central source derived from both the 85.69 GHz continuum and H42α line emission is 4.35 ± 0.25 $M_\odot$ yr^{-1}. This is comparable to what we obtain using the total infrared flux, and it is consistent with the range of SFR values estimated from previous radio recombination line measurements.

(v) The SFR measurements from either previously published radio continuum data or from radio observations of supernovae are a factor of ∼2 higher than what is obtained from the ALMA data. This is potentially related to a combination of calibration issues with the estimates of the SFR based on the radio data or changes in the SFR between 3–40 Myr ago and the present.

(vi) The SFR measurements from *Spitzer* 24 μm and *WISE* 22 μm data are ∼10× lower than the measurements based on the ALMA data as well as the measurement based on the total infrared flux or the measurements based on radio data. This probably occurs because the central starburst is optically thick at mid-infrared wavelengths, which is a condition where the conversion between mid-infrared flux and SFR should no longer yield reliable results.

This analysis not only demonstrates how effective ALMA can be in terms of studying star formation in the centres of starburst galaxies but also how such ALMA observations can be used to cross-check SFR measurements from both infrared and radio data. Mid-infrared flux has been favoured for use as a star formation tracer because of how well the emission has been correlated with other ultraviolet, optical, and near-infrared star formation tracers and because it had been assumed that mid-infrared emission is not affected by the same dust extinction effects as star formation tracers at shorter wavelength. The results here demonstrate that mid-infrared fluxes may not be reliable star formation tracers in compact starbursts. Additional ALMA observations of star-forming regions in other nearby galaxies should be used to explore the reliability of infrared emission as a star formation metric for such dusty systems.

We thank the reviewer for the helpful comments on this paper. GJB and GAF acknowledge support from STFC Grant ST/M000982/1. CD has received funding from the European Research Council under the European Union's Seventh Framework Programme (FP7/2007-2013)/ERC grant agreement no. 307209. CD also acknowledges support from an STFC Consolidated Grant (no. ST/L000768/1). AK acknowledges support by the Collaborative Research Council 956, sub-project A1, funded by the Deutsche Forschungsgemeinschaft (DFG). This paper makes use of the following ALMA data: ADS/JAO.ALMA#2012.1.00912.S. ALMA is a partnership of ESO (representing its member states), NSF (USA) and NINS (Japan), together with NRC (Canada), NSC and ASIAA (Taiwan), and KASI (Republic of Korea), in cooperation with the Republic of Chile. The Joint ALMA Observatory is operated by ESO, AUI/NRAO and NAOJ. This research has made use of the NASA/IPAC Infrared Science Archive, which is operated by the Jet Propulsion Laboratory, California Institute of Technology, under contract with the National Aeronautics and Space Administration. This publication makes use of data products from the *Wide-field Infrared Survey Explorer*, which is a joint project of the University of California, Los Angeles, and the Jet Propulsion Laboratory/California Institute of Technology, and *NEOWISE*, which is a project of the Jet Propulsion Laboratory/California Institute of Technology. *WISE* and *NEOWISE* are funded by the National Aeronautics and Space Administration.

REFERENCES

Altieri B., Vavrek R., eds., 2013, PACS Observer's Manual, Version 2.5.1. Herschel Science Centre, Villanueva de la Cañada, Madrid, Spain

Anantharamaiah K. R., Viallefond F., Mohan N. R., Goss W. M., Zhao J. H., 2000, ApJ, 537, 613

Bendo G. J., Barnes J. E., 2000, MNRAS, 316, 315

Bendo G. J. et al., 2006, ApJ, 645, 134

Bendo G. J., Galliano F., Madden S. C., 2012, MNRAS, 423, 197

Bendo G. J. et al., 2013, MNRAS, 433, 3062

Bendo G. J. et al., 2015a, MNRAS, 448, 135

Bendo G. J., Beswick R. J., D'Cruze M. J., Dickinson C., Fuller G. A., Muxlow T. W. B., 2015b, MNRAS, 450, L80

Bergman P., Aalto S., Black J. H., Rydbeck G., 1992, A&A, 265, 403

Boquien M. et al., 2010, ApJ, 713, 626

Boselli A. et al., 2012, A&A, 540, 54

Brandl B. R. et al., 2006, ApJ, 653, 1129

Brock D., Joy M., Lester D. F., Harvey P. M., Ellis H. B., Jr, 1988, ApJ, 329, 208

Calzetti D. et al., 2005, ApJ, 633, 871

Calzetti D. et al., 2007, ApJ, 666, 870

Calzetti D. et al., 2010, ApJ, 714, 1256

Casey C. M., 2012, MNRAS, 425, 3094

Chou R. C. Y. et al., 2007, ApJ, 670, 116

Ciesla L. et al., 2014, A&A, 565, A128

Condon J. J., 1992, ARA&A, 30, 575

Cunningham M. R., Whiteoak J. B., 2005, MNRAS, 364, 37

Cutri R. M. et al., 2013, Explanatory Supplement to the WISE All-Sky Data Release Products. Infrared Processing and Analysis Center, Pasadena

de Vaucouleurs G., de Vaucouleurs A., Corwin H. G., Buta R. J., Paturel G., Fouque P., 1991, Third Reference Catalogue of Bright Galaxies, Springer-Verlag, Berlin

Dale D. A., Helou G., Magdis G. E., Armus L., Díaz-Santos T., Shi Y., 2014, ApJ, 784, 83

Davies R. D., Dickinson C., Banday A. J., Jaffe T. R., Górski K. M., Davis R. J., 2006, MNRAS, 370, 1125

Díaz-Santos T. et al., 2010, ApJ, 723, 993

Done C., Madejski G. M., Smith D. A., 1996, ApJ, 463, L63

Dowell C. D. et al., 2010, in Oschmann J. M., Jr, Clampin M. C., MacEwen H. A., eds, Proc. SPIE Conf. Ser. Vol. 7731, Space Telescopes and Instrumentation 2010: Optical, Infrared, and Millimeter Wave. SPIE, Bellingham, p. 773136

Draine B. T., 2003, ARA&A, 41, 241

Draine B. T., 2011, Physics of the Interstellar and Intergalactic Medium. Princeton Univ. Press, Princeton, NJ

Engelbracht C. W. et al., 2007, PASP, 119, 994

Fisher D., 1997, AJ, 113, 950

Forbes D. A., Norris R. P., 1998, MNRAS, 300, 757

Galametz M. et al., 2013, MNRAS, 431, 1956

Gordon M. A., 1989, ApJ, 337, 782

Gordon M. A., Walmsley C. M., 1990, ApJ, 365, 606

Gordon K. D. et al., 2005, PASP, 117, 50

Griffin M. J. et al., 2010, A&A, 518, L3

Haarsma D. B., Partridge R. B., Windhorst R. A., Richards E. A., 2000, ApJ, 544, 641

Acknowledgments

The acknowledgments are usually at the end of the conclusions and usually list contributions from other people towards the paper.

People or things that could be mentioned here include:

- The referee
- Other people whom you talked to about the paper
- Observatories
- Software developers
- Websites with useful information
- Scientific grants


268 G. J. Bendo et al.

ACKNOWLEDGEMENTS

We thank the reviewer for the helpful comments on this paper. GJB and GAF acknowledge support from STFC Grant ST/M000982/1. CD has received funding from the European Research Council under the European Union's Seventh Framework Programme (FP7/2007-2013)/ERC grant agreement no. 307209. CD also acknowledges support from an STFC Consolidated Grant (no. ST/L000768/1). AK acknowledges support by the Collaborative Research Council 956, sub-project A1, funded by the Deutsche Forschungsgemeinschaft (DFG). This paper makes use of the following ALMA data: ADS/JAO.ALMA#2012.1.00912.S. ALMA is a partnership of ESO (representing its member states), NSF (USA) and NINS (Japan), together with NRC (Canada), NSC and ASIAA (Taiwan), and KASI (Republic of Korea), in cooperation with the Republic of Chile. The Joint ALMA Observatory is operated by ESO, AUI/NRAO and NAOJ. This research has made use of the NASA/IPAC Infrared Science Archive, which is operated by the Jet Propulsion Laboratory, California Institute of Technology, under contract with the National Aeronautics and Space Administration. This publication makes use of data products from the *Wide-field Infrared Survey Explorer*, which is a joint project of the University of California, Los Angeles, and the Jet Propulsion Laboratory/California Institute of Technology, and *NEOWISE*, which is a project of the Jet Propulsion Laboratory/California Institute of Technology. *WISE* and *NEOWISE* are funded by the National Aeronautics and Space Administration.

References

The references section presents a list of all the papers that are mentioned in the text.

It generally makes people feel better if you reference their papers, so it is OK to have lots of references.

Also, when appropriate, try to include references to online documents (such as observatory or instrument manuals) and textbooks as well as scientific articles.

References

The references section presents a list of all the papers that are mentioned in the text.

It generally makes people feel better if you reference their papers, so it is OK to have lots of references.

Also, when appropriate, try to include references to online documents (such as observatory or instrument manuals) and textbooks as well as scientific articles.

References

The references section presents a list of all the papers that are mentioned in the text.

It generally makes people feel better if you reference their papers, so it is OK to have lots of references.

Also, when appropriate, try to include references to online documents (such as observatory or instrument manuals) and textbooks as well as scientific articles.

Appendices

The appendices include supplementary information.

This is often a good place to put the following:

- Extra figures or tables
- Information on deriving equations
- Additional analyses that help support the results from the main analysis section

Prescott M. K. M. et al., 2007, ApJ, 668, 182
Rice W., Lonsdale C. J., Soifer B. T., Neugebauer G., Kopan E. L., Lloyd L. A., de Jong T., Habing H. J., 1988, ApJS, 68, 91
Rieke G. H. et al., 2004, ApJS, 154, 25
Roberts W. W., 1969, ApJ, 158, 123
Roussel H., 2013, PASP, 125, 1126
Roussel H. et al., 2001, A&A, 372, 406
Rowan-Robinson M. et al., 2010, MNRAS, 409, 2
Roy R. et al., 2011, ApJ, 736, 76
Saha A., Thim F., Tammann G. A., Reindl B., Sandage A., 2006, ApJS, 165, 108
Sauvage M., Thuan T. X., 1992, ApJ, 396, L69
Sauvage M. et al., 2010, A&A, 518, L64
Schlafly E. F., Finkbeiner D. P., 2011, ApJ, 737, 103
Schmidt M., 1959, ApJ, 129, 243
Sheth K. et al., 2010, PASP, 122, 1397
Shetty R., Kauffmann J., Schnee S., Goodman A. A., Ercolano B., 2009, ApJ, 696, 2234
Silva L., Granato G. L., Bressan A., Danese L., 1998, ApJ, 509, 103
Smith M. W. L., 2012, PhD thesis, Cardiff University
Smith M. W. L. et al., 2010, A&A, 518, L51
Smith M. W. L. et al., 2012a, ApJ, 748, 123
Smith M. W. L. et al., 2012b, ApJ, 756, 40
Spitzer Science User Support and Instrument Teams, IRSA Science User Support Team, 2012, Spitzer Data Analysis Cookbook, Version 5.0.1, Spitzer Science Center, Pasadena
Storey P. J., Zeippen C. J., 2000, MNRAS, 312, 813
Tabatabaei F. S. et al., 2014, A&A, 561, 95
Thomas G., Haraki M. O., Coudreau N., Hallet N., Martin J.-M., 2007, A&A, 465, 71
Tonry J. L., Dressler A., Blakeslee J. P., Ajhar E. A., Fletcher A. B., Luppino G. A., Metzger M. R., Moore C. B., 2001, ApJ, 546, 681
Tully R. B., Rizzi L., Shaya E. J., Courtois H. M., Makarov D. I., Jacobs B. A., 2009, AJ, 138, 323
Valtchanov I., ed., 2014, The Spectral and Photometric Imaging Receiver (SPIRE) Handbook, Version 2.5. *Herschel* Science Centre, Villanueva de la Cañada, Madrid
Werner M. W. et al., 2004, ApJS, 154, 1
Wright E. L. et al., 2010, AJ, 140, 1868
Xilouris E. M., Byun Y. I., Kylafis N. D., Paleologou E. V., Papamastorakis J., 1999, A&A, 344, 868
Xilouris E. M. et al., 2012, A&A, 543, 74
Zhu Y.-N., Wu H., Cao C., Li H.-N., 2008, ApJ, 686, 155

APPENDIX A: COMPARISONS OF Hα AND 24 μm EMISSION

Multiple authors (e.g. Calzetti et al. 2005, 2007; Prescott et al. 2007) have found a good correspondence between Hα and 24 μm emission from compact sources within nearby galaxies. However, it is possible for diffuse dust to produce 24 μm emission, and this diffuse emission will not necessarily correspond to Hα emission (Kennicutt et al. 2009). Additionally, the ratio of Hα to 24 μm emission may vary with metallicity as well. To examine whether this could affect our analysis, we compared uncorrected Hα and 24 μm emission measured within the 24 arcsec binned data in our analysis, as we also compared the correlations of the 160/250 and 250/350 μm ratios to the uncorrected Hα, corrected Hα, and 24 μm emission. We selected data for 24 arcsec bins where both the uncorrected Hα and 24 μm emission were measured at the 3σ level and where the data otherwise met the criteria for use in the analysis in Section 5; the data meeting the criteria for analysis on the 250/350 μm ratio were also used for calculating correlation coefficients for the relations between the uncorrected Hα and 24 μm emission. These selection criteria are necessary for directly comparing Hα and 24 μm emission but may cause the resulting coefficients to differ slightly (<0.05) from the coefficients in Table 4 listed for the same relations.

The weighted correlation coefficients from this analysis are presented in Table A1. First, we can see that while the uncorrected Hα and 24 μm data are often strongly correlated, the correlation coefficients do not always equal 1, and some of the values drop to <0.80. Although the Hα and 24 μm emission is clearly correlated, enough scatter exists that swapping one for the other could potentially change the relations we see when comparing these star formation tracers to the 160/250 and 250/350 μm surface brightness ratios. Further analysis to understand these variations and, in particular, to identify whether they are associated with other properties of the ISM (such as the gas-to-dust ratio or metallicity), would be useful, but this is beyond the scope of this paper.

In the comparison of the different star formation tracers to the infrared surface brightness ratios, we generally found that the correlations with the uncorrected Hα emission were the weakest and the correlations with the 24 μm emission were strongest. The correlation coefficients for the relations using the extinction-corrected Hα emission usually fell between the other two, which is expected given that the corrected Hα emission is based on a combination of the uncorrected Hα and 24 μm emission. The coefficients for the relations with the corrected Hα emission are sometimes higher than for the corresponding relations with the 24 μm emission, but with one exception (the relations for the 160/250 μm ratio for NGC 5364, where all coefficients are <0.50), the difference never exceeds 0.05.

For 15 of the 22 galaxies, the weighted correlation coefficients were ≥0.05 higher for at least one (but usually two) of the relations between the far-infrared ratios and the 24 μm surface brightness than for the corresponding relations between the ratios and the uncorrected Hα intensity. NGC 3031, 3953, 4548, and 4725 are all cases where we masked emission in the centres of the Hα image that we determined was incompletely subtracted continuum emission (based on the diffuse appearance of the emission and the presence of artefacts similar to what was seen for foreground stars). We did not remove any 24 μm emission from these regions, which probably originates from dust heated in part or completely by the evolved stellar population, particularly the bulge stars. If the emission at 160–350 μm also originates from dust heated by the evolved stellar population, then the 160/250 and 250/350 μm ratios may naturally correlate with the 24 μm band very well within these central regions, and the correlation coefficients for the overall relations between the far-infrared ratios and 24 μm emission will be higher than the relations between the ratios and the Hα emission. We therefore should disregard the 'improved' relation found between the ratios and the 24 μm emission in these four galaxies. Of the remaining 11 galaxies where a significantly stronger correlation is found between either ratio and 24 μm emission, the major question is whether changing the star formation tracer would alter our interpretation of whether the far-infrared ratios were more strongly affected by star-forming regions or the evolved stellar population as presented in Section 5. NGC 628, 925, 3184, 3938, 4303, 5364, and 7793 are the only remaining cases where this could be an issue. In these seven galaxies, we would be more likely to infer that dust heating by star-forming regions is less significant when using the uncorrected Hα emission or more significant when using the 24 μm emission. This may still be caused in part by 24 μm emission from dust heated by the diffuse ISRF.

How to read papers

- It is frequently sufficient to just read the **Abstract**, which should contain a basic summary of the paper.
- For slightly more information, look at the **Figures**, the **Conclusion**, and possibly some derived **Equations**.
- For more in-depth information, read the entire paper (but skip the **Data** section).
- For background information and references to other papers, read the **Introduction**.
- To simply get some numbers (e.g. distances to objects), look up the data in a **Table**.
- Refer to the **Data** section when trying to reproduce someone's images, spectra, or measurements.

LaTeX

LaTeX

LaTeX is a typesetting system used for creating many professional journal articles.

The files look like text files with additional inserted comments.

Additional commands are specified in the text after backslashes (\).

Math symbols are specified within dollar signs ($).

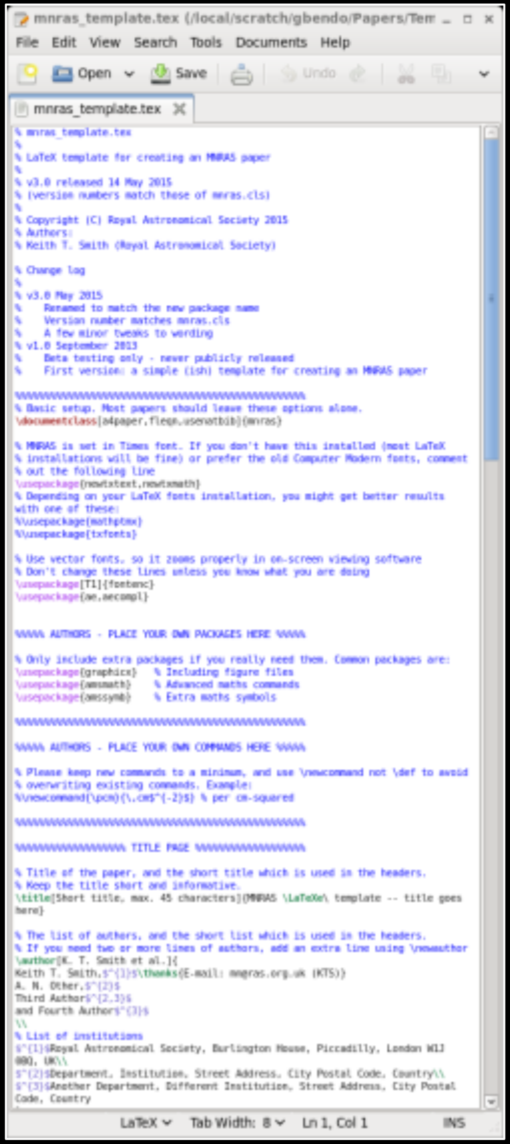

A LaTeX document usually includes the following lines:

- **\documentclass**
- Additional header statements, including the following:
  - **\usepackage**
  - **\title**
  - **\author**
  - **\date**
- **\begin{document}**
- **\maketitle**
- The text of the paper itself
- **\end{document}**

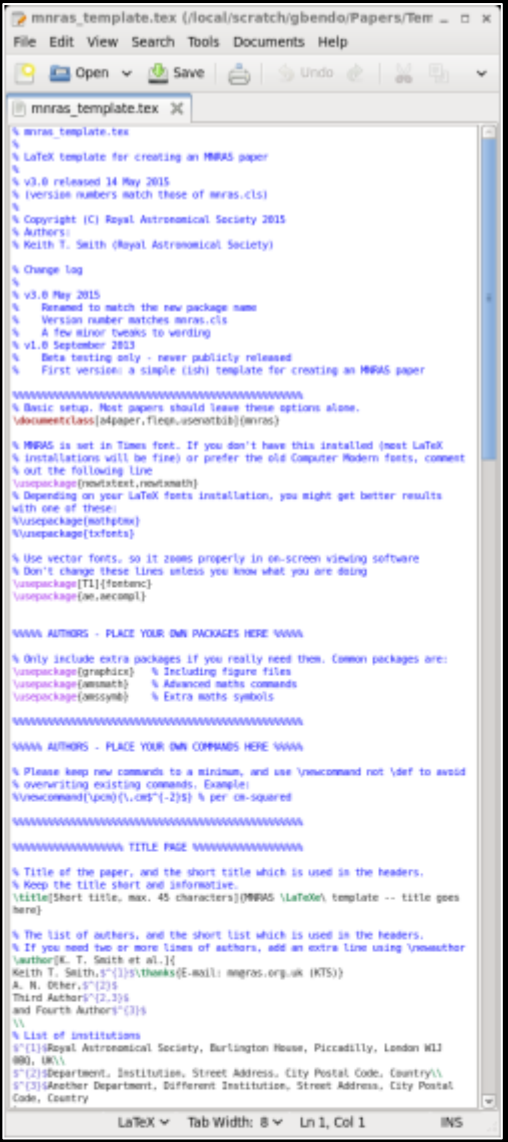

Templates

The major journals each have templates available at the following locations:

- **A&A**: www.aanda.org/author-information/latex-issues/latex-examples
- **AJ**: journals.aas.org/authors/aastex.html
- **ApJ**: journals.aas.org/authors/aastex.html
- **MNRAS**: ctan.org/tex-archive/macros/latex/contrib/mnras

You may need to write your PhD thesis in LaTeX as well. Other students at your home institution may have templates for this.

BibTeX

BibTeX is a useful way for storing citations material for papers.

When a BibTeX file is compiled with a LaTeX file, it will automatially generate a list of references in the needed format for the journal.

BibTeX files can include a list of citations used in multiple papers. The resulting reference list for any LaTeX paper will only include the papers cited in the LaTeX file.

ADS Abstracts has an option to generate entries in BibTeX format.


```
@ARTICLE{1974ARA&A..12..279Z,
  author = {{Zuckerman}, B. and {Palmer}, P.},
  year = 1974,
  title = {{Radio radiation from interstellar molecules}},
  journal = {\araa},
  volume = 12,
  pages = {279--313},
  url = {http://adsabs.harvard.edu/cgi-bin/nph-bib_query?bibcode=1974ARA%
26A..12..279Z&db_key=AST},
  adsnote = {Provided by the NASA Astrophysics Data System}
}

@ARTICLE{2000A&AS..143...85A,
    author = {{Accomazzi}, A. and {Eichhorn}, G. and {Kurtz}, M.~J. and {Grant},
C.~S. and
        {Murray}, S.~S.},
    title = "{The NASA Astrophysics Data System: Architecture}",
    journal = {\aaps},
    year = 2000,
    month = apr,
    volume = 143,
    pages = {85--109},
    url = {http://adsabs.harvard.edu/cgi-bin/nph-bib_query?bibcode=2000A%
26AS..143...85A&db_key=AST},
}

@ARTICLE{2000A&AS..143...61E,
    author = {{Eichhorn}, G. and {Kurtz}, M.~J. and {Accomazzi}, A. and {Grant},
C.~S. and
        {Murray}, S.~S.},
    title = "{The NASA Astrophysics Data System: The search engine and its user
interface}",
    journal = {\aaps},
    year = 2000,
    month = apr,
    volume = 143,
    pages = {61--83},
}
```

LaTeX editors

LaTeX documents can be edited using simple text editors (emacs, gedit, notepad, etc). The documentgs can then be compiled at the command line.

Windows and Mac have special packages for editing LaTeX documents. I use the following:

- TeXworks (Windows)
  www.tug.org/texworks/
- TeXShop (Mac)
  pages.uoregon.edu/koch/texshop/

LaTeX documents can also be created online using Overleaf (www.overleaf.com).

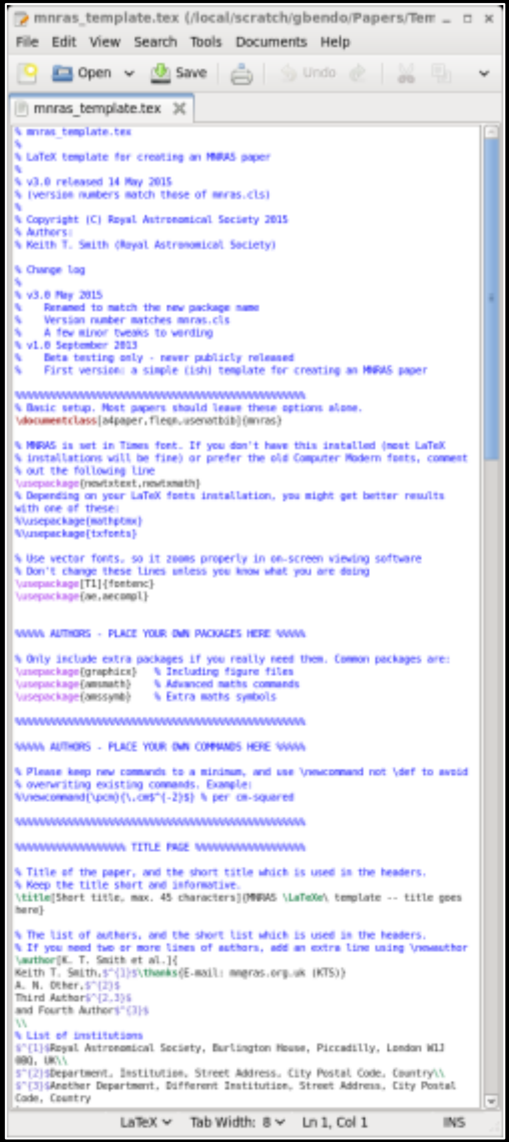

LaTeX editors

LaTeX documents can be edited using simple text editors (emacs, gedit, notepad, etc). The documentgs can then be compiled at the command line.

Windows and Mac have special packages for editing LaTeX documents. I use the following:

- TeXworks (Windows) www.tug.org/texworks/
- TeXShop (Mac) pages.uoregon.edu/koch/texshop/

LaTeX documents can also be created online using Overleaf (www.overleaf.com).

LaTeX editors

LaTeX documents can be edited using simple text editors (emacs, gedit, notepad, etc). The documentgs can then be compiled at the command line.

Windows and Mac have special packages for editing LaTeX documents. I use the following:

- TeXworks (Windows)
  www.tug.org/texworks/
- TeXShop (Mac)
  pages.uoregon.edu/koch/texshop/

LaTeX documents can also be created online using Overleaf (www.overleaf.com).

LaTeX editors

LaTeX documents can be edited using simple text editors (emacs, gedit, notepad, etc). The documentgs can then be compiled at the command line.

Windows and Mac have special packages for editing LaTeX documents. I use the following:

- TeXworks (Windows) www.tug.org/texworks/
- TeXShop (Mac) pages.uoregon.edu/koch/texshop/

LaTeX documents can also be created online using Overleaf (www.overleaf.com).

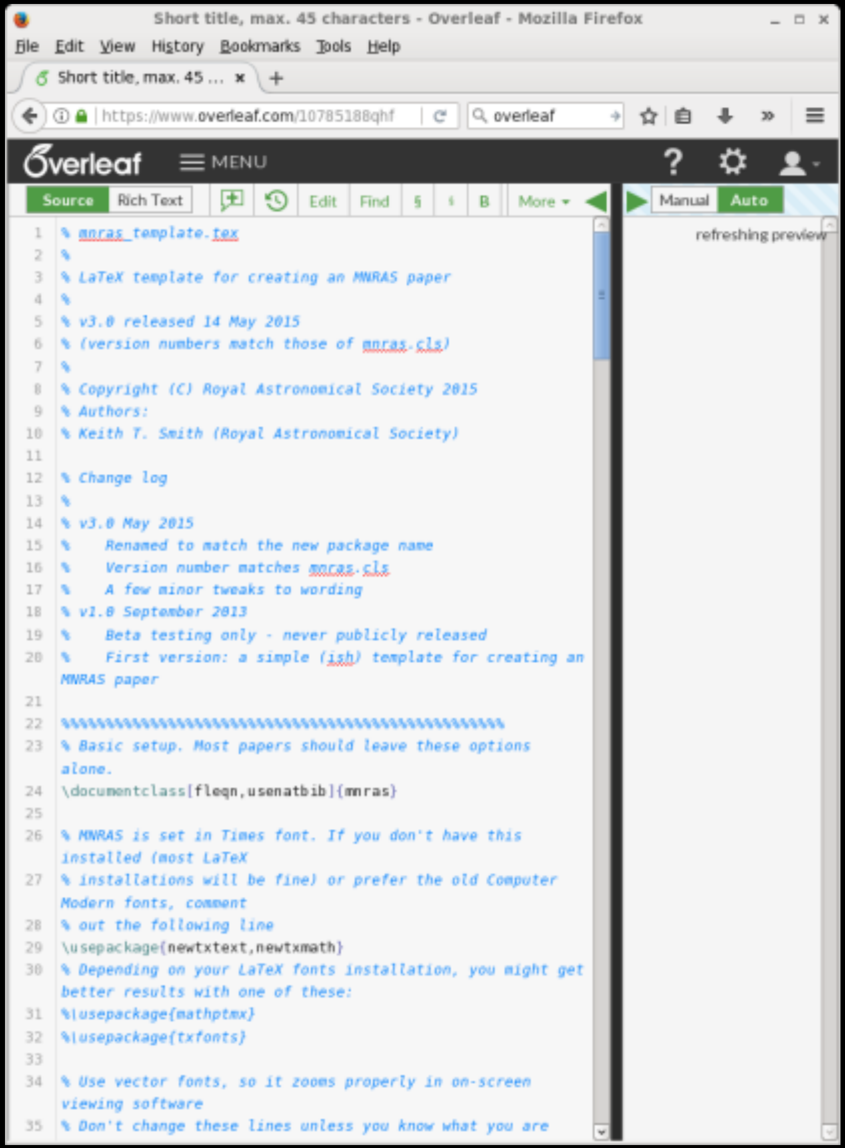

Practical Process for Paper Writing

The timeline for writing a paper before submission usually proceeds as follows:

2 months – 2 years: The first author starts writing the paper. After some time, a complete paper is ready.

2 weeks – 3 months: The paper is reviewed by one or more people, who provide comments on what needs to be changed in the paper.

1 – 3 months: The first author makes changes to the paper.

The prior two steps repeat until everyone has read the paper and everyone stops generating comments on major changes that need to be made to the paper.

The timeline for a paper after submission is as follows:

1 month: The editors send the paper to a referee (also called a reviewer), who writes comments that are sent back to you.

1 week – 6 months: The first author makes changes to the paper.

The first two steps repeat until the reviewer is happy with the paper, at which time the paper is accepted for publication.

After the paper is accepted, the following should happen:

- A copy of the paper should be posted on arXiv.
- Any copyright forms need to be completed and returned to the journal.
- The proofs (the final form of the paper) should be reviewed and edited by the first author.
- Any page charges need to be paid.

Publication Statistics

Any researcher’s publication record can be measured through various metrics, including the following:

- Total number of refereed papers
- Total number of refereed first-author papers
- Total citations to (all or first-author) papers
- Normalized citations to papers (each paper’s citations is normalized by the number of authors)
- h-index (the number n where n papers have at least n citations)

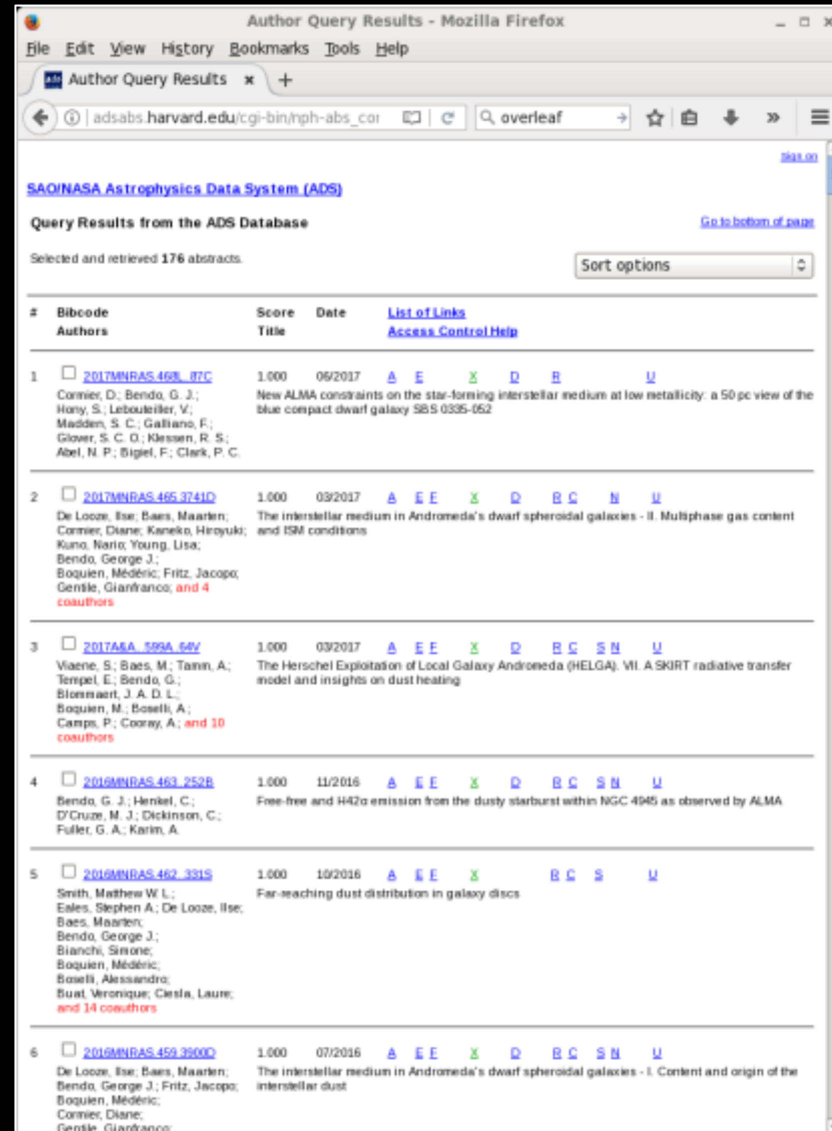

Any researcher's publication record can be measured through various metrics, including the following:

- Total number of refereed papers
- Total number of refereed first-author papers
- Total citations to (all or first-author) papers
- Normalized citations to papers (each paper's citations is normalized by the number of authors)
- h-index (the number n where n papers have at least n citations)

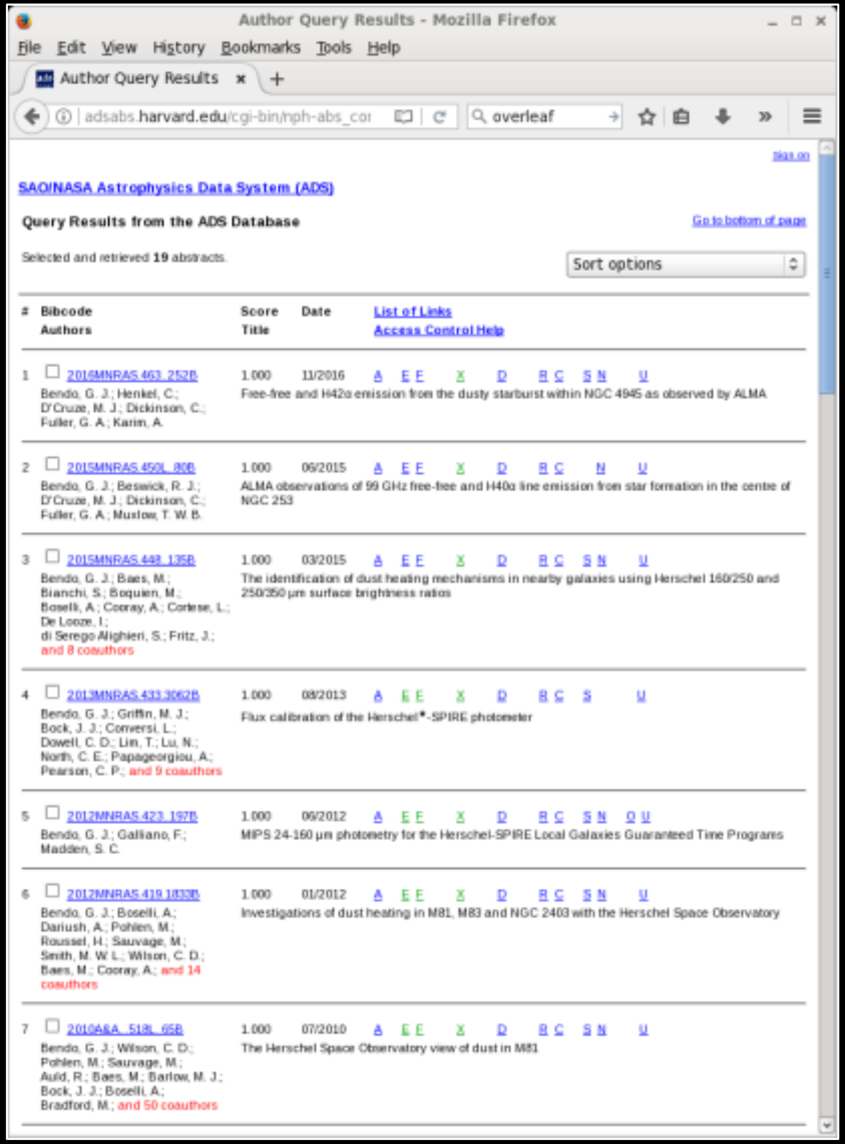

Any researcher's publication record can be measured through various metrics, including the following:

- Total number of refereed papers
- Total number of refereed first-author papers
- Total citations to (all or first-author) papers
- Normalized citations to papers (each paper's citations is normalized by the number of authors)
- h-index (the number n where n papers have at least n citations)

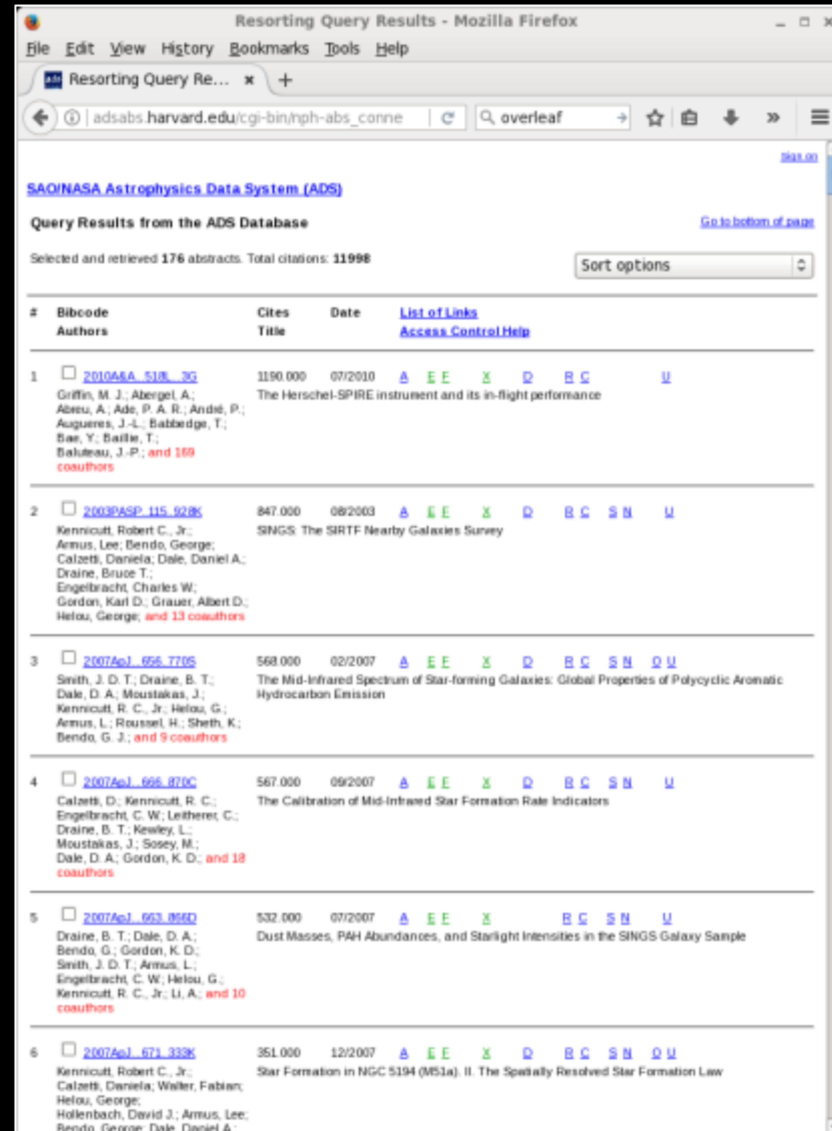

Any researcher's publication record can be measured through various metrics, including the following:

- Total number of refereed papers
- Total number of refereed first-author papers
- Total citations to (all or first-author) papers
- Normalized citations to papers (each paper's citations is normalized by the number of authors)
- h-index (the number n where n papers have at least n citations)

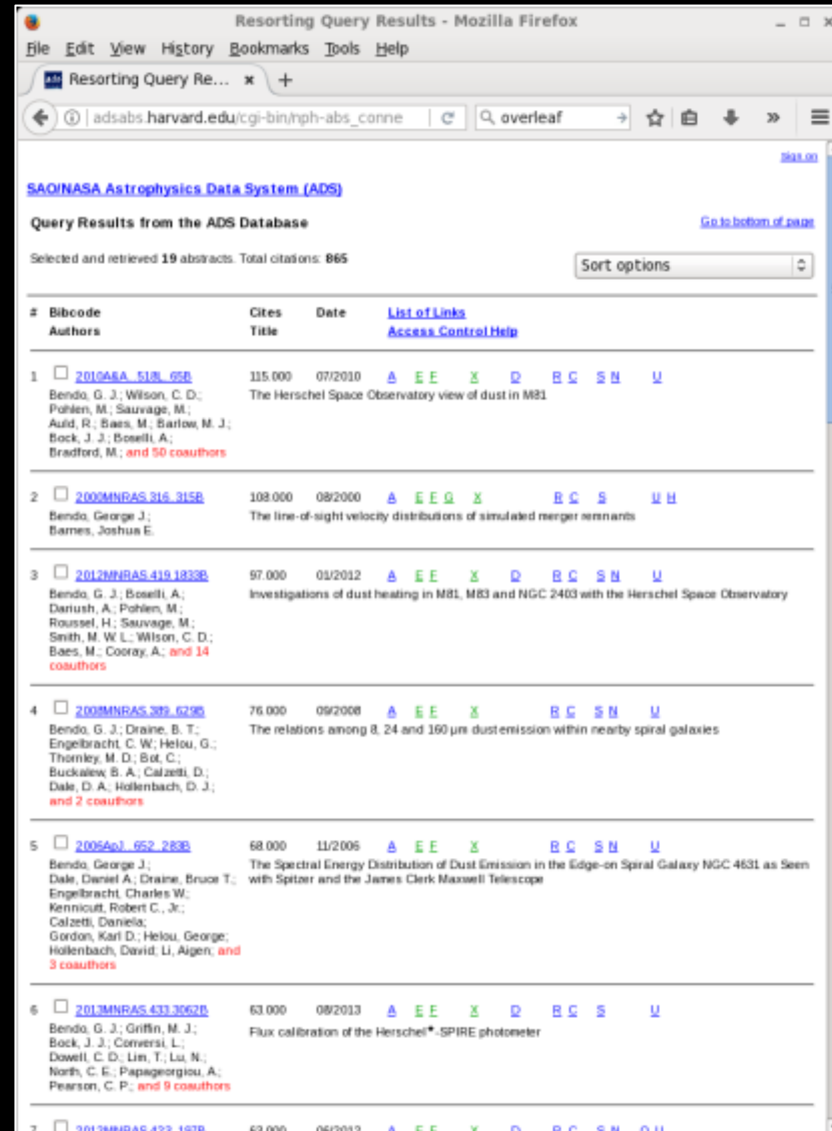

Any researcher's publication record can be measured through various metrics, including the following:

- Total number of refereed papers
- Total number of refereed first-author papers
- Total citations to (all or first-author) papers
- Normalized citations to papers (each paper's citations is normalized by the number of authors)
- h-index (the number n where n papers have at least n citations)

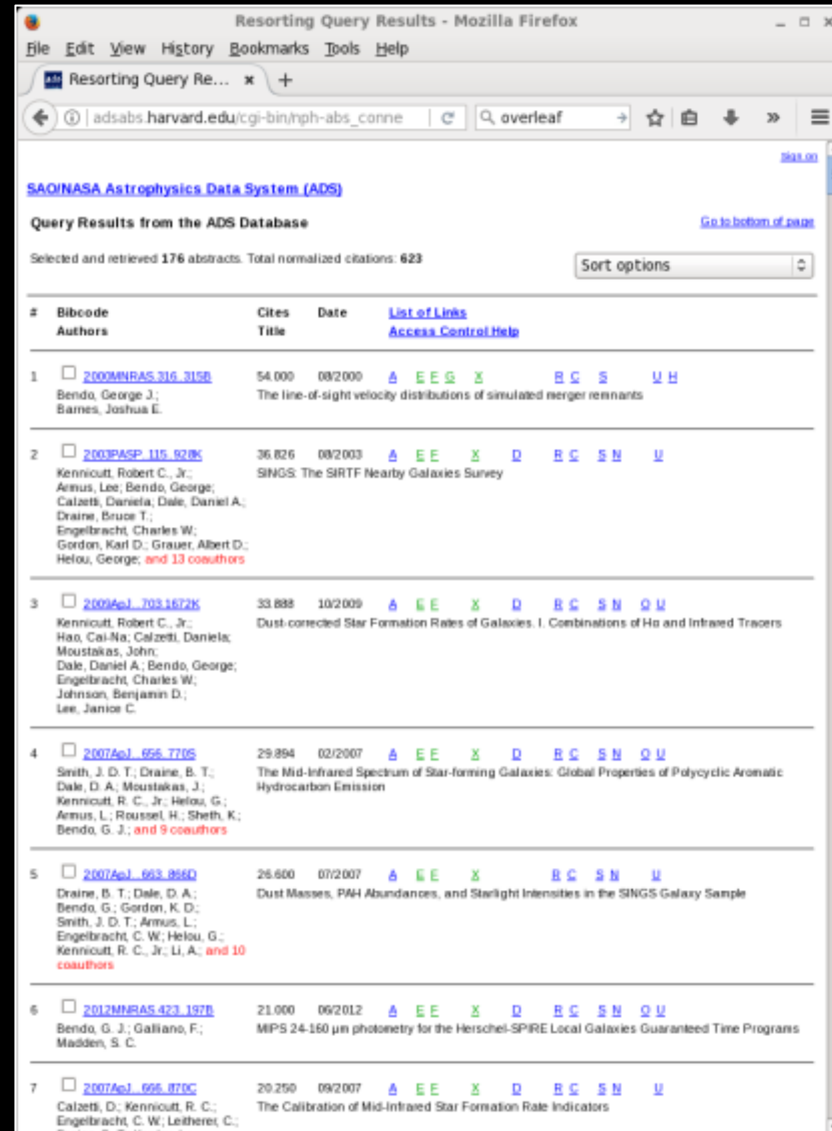

Any researcher's publication record can be measured through various metrics, including the following:

- Total number of refereed papers
- Total number of refereed first-author papers
- Total citations to (all or first-author) papers
- Normalized citations to papers (each paper's citations is normalized by the number of authors)
- h-index (the number n where n papers have at least n citations)

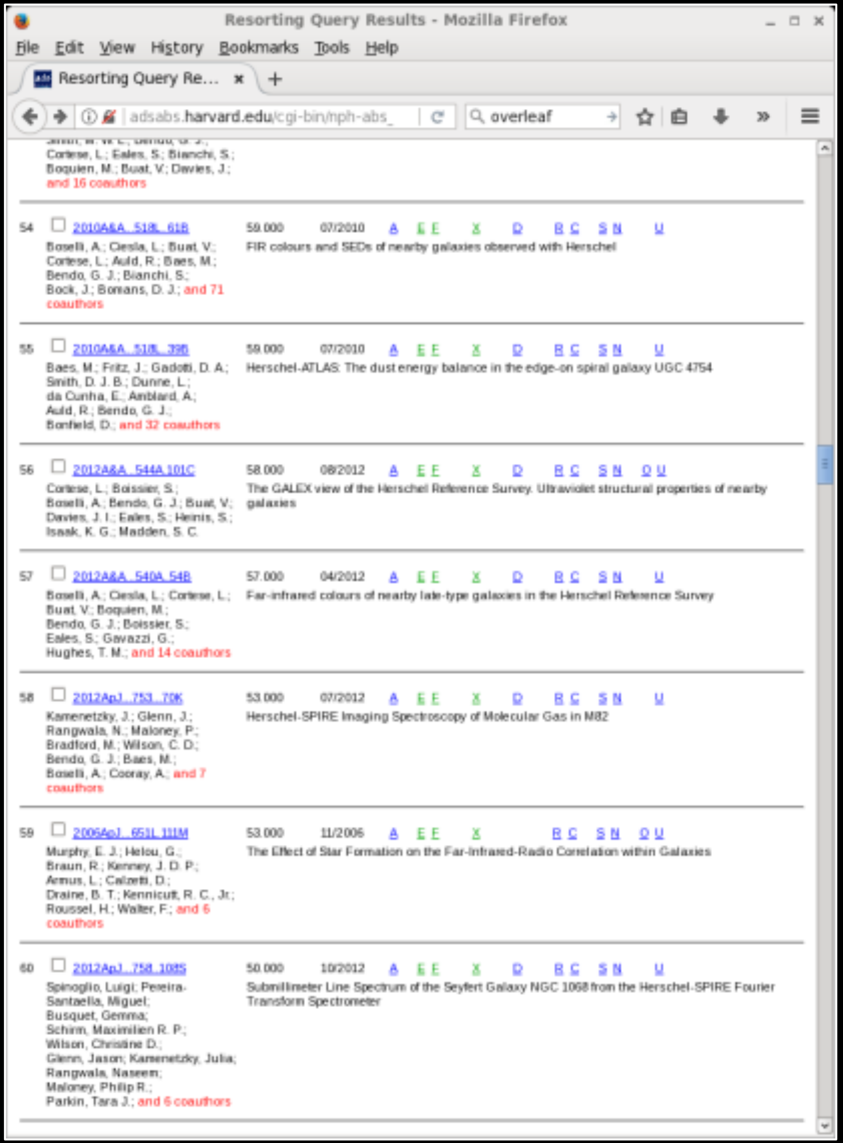

These metrics do not necessarily indicate that someone is a good or bad researcher.

- Some people could churn out a lot of papers that cite each other but otherwise achieve very little.

- Some senior researchers get more involved in grant writing, management, and/or teaching and do not publish many papers.

- Some researchers focus more on promoting their students' and postdocs' work and do not publish many first author papers.

- Some researchers work more on behind-the-scenes activities (e.g. instrument development and support) and may only be recognized when that effort becomes publicly visible.

You can drive up your publication statistics in a few ways.

- Publish lots of papers.
- Cite yourself frequently.
- Ask other people to cite you.
- Work in a large collaboration where people use your results.
- Publicly release your data.
- Present your results at conferences.
- Produce press releases based on your papers.